RESEARCH ON ENERGY ABSORBING STRUCTURES. PART XI

Bernard Mazelsky, et al

ARA, Incorporated

Prepared for:

Air Force Office of Scientific Research

March 1973

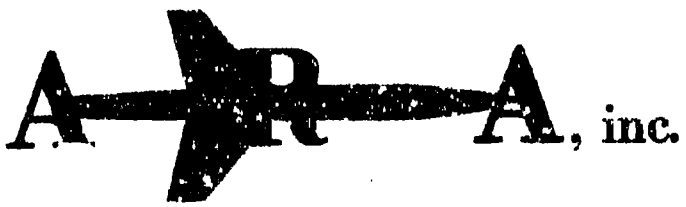

AEROSPACE RESEARCH ASSOCIATES

2017 West Garvey Avenue • West Covina, California • Tel. 962-1045

DOCUMENT CONTROL DATA - R & D

(Security classification of title, body of abstract and indexing annotation must be entered when the overall report is classified)

1. ORIGINATING ACTIVITY (Corporate author) AEROSPACE RESEARCH ASSOCIATES, INC. 7 WEST GARVEY AVENUE WEST COVINA, CALIFORNIA 91790	2a. REPORT SECURITY CLASSIFICATION UNCLASSIFIED 2b. GROUP

3. REPORT TITLE

RESEARCH ON ENERGY ABSORBING STRUCTURES, PART XI

4. DESCRIPTIVE NOTES (Type of report and inclusive dates)

Scientific Interim

5. AUTHOR(S) (First name, middle initial, last name)

BERNARD MAZELSKY TUNG HUA LIN SHENG-RONG LIN SHIH-CHANG LIU

6. REPORT DATE 1973		7a. TOTAL NO. OF PAGES 54 60	7b. NO. OF REFS
8a. CONTRACT OR GRANT NO. F44620-71-C-0043		9a. ORIGINATOR'S REPORT NUMBER(S)	
b. PROJECT NO.	9782-02	ARA Report No. 154	
c.	61102F	9b. OTHER REPORT NO(S) (Any other numbers that may be assigned this report)	
d.	681307	AFOSR - TR - 73 - 0775	

10. DISTRIBUTION STATEMENT

Approved for public release; distribution unlimited

11. SUPPLEMENTARY NOTES TECH, OTHER	12. SPONSORING MILITARY ACTIVITY AF Office of Scientific Research (NAM) 1400 Wilson Boulevard Arlington, Virginia 22209

13. ABSTRACT

A numerical method for analyzing large deflections of shells of revolution under axisymmetric loading with arbitrary creep characteristics is given. Creep strain is treated as an equivalent external loading. Two nonlinear differential equations similar to Reissner's equations are presented and solved by the iterative scheme and the finite difference approximation. The multiaxial stress-strain-time relationship is formulated from the empirical uniaxial curve based on the second deviated stress and strain invariants. Examples are given for a corrugated tube subject to an axial load at an elevated temperature. The results show the nonlinear effects due to finite strain and creep strain. The method shown may also be applied to axisymmetric shells subject to thermal and plastic strains. A face-centered-cubic polycrystal under cyclic loading is considered. It is shown that slip in the primary slip system causes the resolved shear stress in a second slip system to increase to the critical value and then this second slip system slides. Slip in this second slip system greatly increases the rate of the local plastic strain build-up in the primary slip system. Hence the occurence of the second active slip system may greatly increase rate of extrusion and intrusion commonly observed in face-centered-cubic metals.

DD FORM 1 NOV 1473

1b

UNCLASSIFIED

Security Classification

KEY WORDS	ROLE	WT	ROLE	WT	ROLE	WT
CREEP STRAIN						
LARGE DEFLECTION THEORY						
AXISYMMETRIC THIN SHELL						
SHELL OF REVOLUTION						
CORRUGATED TUBE						
FATIGUE CRACK NUCLEATION						
PLASTIC STRAIN						
MICROSTRESS						
RESOLVED SHEAR STRESS						
SLIP LINE						
SECONDARY SLIP SYSTEM						
CYCLIC LOADING						
FACE-CENTERED-CUBIC CRYSTAL						
PLASMA SPRAY METAL COATING						

UNCLASSIFIED
Security Classification

Annual Report on Research on Energy Absorbing Structures

Part XI

Contract Number: F44620-71-C-0043

ARA Report No. 154

Prepared for
Air Force Office of Scientific Research
Arlington, Virginia 22209

"APPROVED FOR PUBLIC RELEASE; DISTRIBUTION UNLIMITED"

March 1973

FOREWORD

The research work described in this report was performed by ARA, Inc., West Covina, California, for the Mechanics Division, Directorate of Engineering Services, Air Force Office of Scientific Research, Arlington, Virginia 22209, under Contract Number F44620-71-C-0043. The research represents the eleventh year program and is part of a continuing effort in the study of inelastic theory of structures with large deflections and fatigue damage in metals due to cyclic loadings. The Project Engineer was Dr. Jacob Pomerantz.

The studies presented began 1 February 1972 and were concluded 1 February 1973. Mr. Bernard Mazelsky was the Principal Investigator. The main contributor to the study was Dr. S. R. Lin of ARA, Inc. Mr. S. C. Liu of ARA, Inc. participated in this program. Professor T. H. Lin of UCLA served as consultant on the analytical study.

TABLE OF CONTENTS

Part A

Large Deflection of Axisymmetric Shell with Creep Strain

I SUMMARY

A numerical method for analyzing large deflections of shells of revolution under axisymmetric loading with arbitrary creep characteristics is given. Creep strain is treated as an equivalent external loading. Two nonlinear differential equations similar to Reissner's equations are presented and solved by the iterative scheme and the finite difference approximation. The multiaxial stress-strain-time relationship is formulated from the empirical uniaxial curve based on the second deviated stress and strain invariants. Examples are given for a corrugated tube subject to an axial load at an elevated temperature. The results show the nonlinear effects due to finite strain and creep strain. The method shown may also be applied to axisymmetric shells subject to thermal and plastic strains.

II INTRODUCTION

Recent interest in the design and fabrication of structures at elevated temperatures has led to the investigation of creep effects in a number of structural configurations. Analyses of beams [1], columns [2-4], and plates [5-8] with creep have been shown. The large deflection of rectangular plates with nonlinear strain-hardening creep, was given by Ho and Lin [9]. Recently the study of the

inelastic behavior of shells has become an area of increasing interest. The large inelastic deformation of spherical shells has been studied by Pian and his associates [10,11]. The detailed method of calculating the stresses and deflections of a corrugated tube with finite strain and nonlinear creep has not been found in the literature. The present study develops such a method to calculate strasses at different points of an axisymmetric shell under axisymmetric loading such as corrugated tubes with arbitrary creep characteristics.

Inelastic strain gradient has been shown to have an equivalent effect as that caused by a distributed body force on the structure [12]. This method of equivalent load has been used in many analyses of inelastic bending of plates [7-9, 13, 14]. In the present study, the sume concept is applied to the analysis of a corrugated tube undergoing very large deflection with creep strain. The nonlinear governing equations are solved by an iterative procedure. The numerical results demonstrate the necessary convergence properties of this method.

III BASIC EQUATIONS

Using cylindrical coordinates r, θ, z, the middle surface of a shell of revolution may be represented by the parametric equations:

$$\begin{cases} r = r(\xi) \\ z = z(\xi) \end{cases} \tag{1}$$

so that the parameter ξ together with the polar angle θ are coordinates on the middle surface. The equation of the deformed middle surface is taken in the form

$$\begin{cases} r = r_o + u \\ \varphi = \varphi_o + \beta \\ z = z_o + w \end{cases} \tag{2}$$

where subscript "o" denotes the quantity referring to the undeformed state. The displacements u and w are components in the radial direction r and axial direction z of the shell, respectively, and β is the change of slope angle Φ of the meridians with respect to the z - axis as shown in Figure 1. From geometry, we have

$$\begin{cases} \frac{dr}{dS} = \cos\Phi \\ \frac{dz}{dS} = \sin\Phi \end{cases} \tag{3}$$

where S is the distance measured along the meridian. The principal strains at the middle surface, in the tangential and circumferential directions, are given as

$$\begin{cases} e_{\varphi_m} = \frac{dS}{dS_o} - 1 \\ e_{\theta_m} = \frac{u}{r_o} \end{cases} \tag{4}$$

The immediate consequence of the definitions of the components e_{φ_m} and e_{θ_m} is the compatibility equation

$$\alpha_o \varepsilon_{\varphi_m} \cos\Phi - (r_o e_{\theta_m})' = \alpha_o (\cos\varphi_o - \cos\Phi) \tag{5}$$

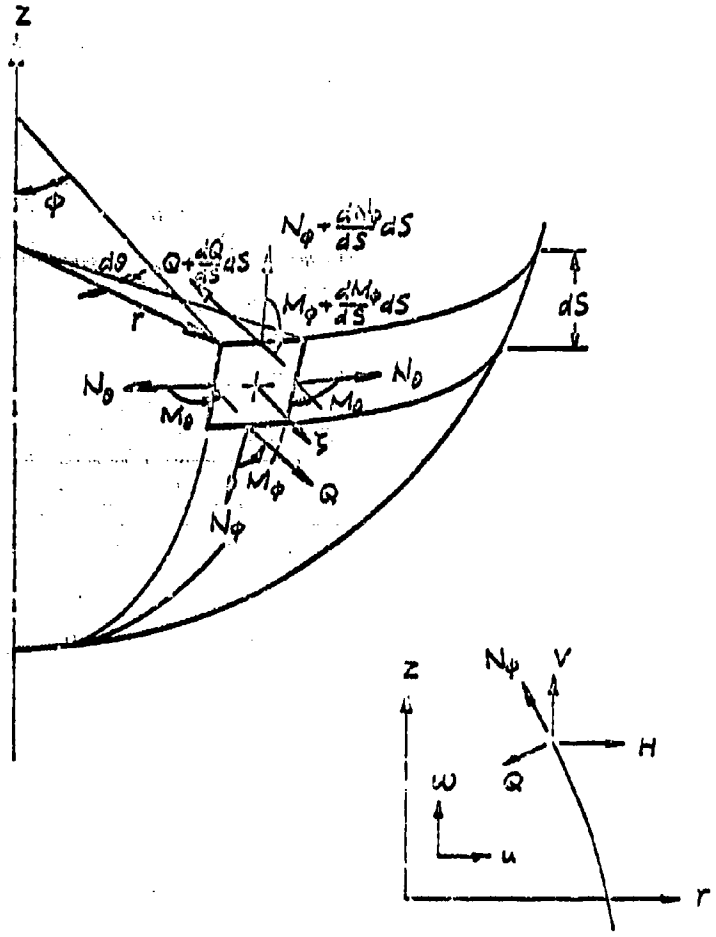

Figure 1. Nomenclature for Shell Element

where prime denotes differentiation with respect to ξ and where α_o is given in the form

$$\alpha_o = \frac{dr_o}{d\xi} \qquad \text{or} \qquad \alpha = \frac{dr}{d\xi} \tag{6}$$

Let ζ be the distance along the normal to the deformed shell surface from the middle surface. By using Kirchoff's assumption that normals to the middle surface remain normal to the deformed middle surface, the strain-displacement relation may be written as

$$\begin{cases} e_\phi = e_{\phi_m} + \zeta \left(\frac{\Phi'}{\alpha} - \frac{\Phi_o'}{\alpha_o} \right) \\ e_\theta = e_{\theta_m} + \zeta \left(\frac{\sin\Phi}{r} - \frac{\sin\Phi_o}{r_o} \right) \end{cases} \tag{7}$$

By Hooke's law, we have the stresses along principal directions ϕ and θ.

$$\begin{cases} \sigma_\phi = \frac{E}{1-\nu^2} \left(e_\phi + \nu e_\theta - e_\phi'' - \nu e_\theta'' \right) \\ \sigma_\theta = \frac{E}{1-\nu^2} \left(e_\theta + \nu e_\phi - e_\theta'' - \nu e_\phi'' \right) \end{cases} \tag{8}$$

where E is Young's modulus, ν is Poisson's ratio, and, e_ϕ'' and e_θ'' are plastic components (including creep) of principal strains. From Equations (7) and (8), the stress resultants and the sectional moments are found as

$$\begin{cases} N_\phi = \frac{Et}{1-\nu^2} \left(e_{\phi_m} + \nu e_{\theta_m} \right) - N_{\phi_I} \\ N_\theta = \frac{Et}{1-\nu^2} \left(e_{\theta_m} + \nu e_{\phi_m} \right) - N_{\theta_I} \\ M_\phi = \frac{Et^3}{12(1-\nu^2)} \left[\frac{\Phi_o'}{\alpha_o} - \frac{\Phi'}{\alpha} + \nu \left(\frac{\sin\Phi_o}{r_o} - \frac{\sin\Phi}{r} \right) \right] + M_{\phi_I} \\ M_\theta = \frac{Et^3}{12(1-\nu^2)} \left[\frac{\sin\Phi_o}{r_o} - \frac{\sin\Phi}{r} + \nu \left(\frac{\Phi_o'}{\alpha_o} - \frac{\Phi'}{\alpha} \right) \right] + M_{\theta_I} \end{cases} \tag{9}$$

where t is the thickness of the shell, and the inelastic terms with subscript " I " are defined as follows

$$\begin{cases} N_{\phi_I} = \frac{E}{1-\nu^2}\int_{-t/2}^{t/2} (e_\phi^p + \nu e_\theta^p)\, d\zeta \\ N_{\theta_I} = \frac{E}{1-\nu^2}\int_{-t/2}^{t/2} (e_\theta^p + \nu e_\phi^p)\, d\zeta \\ M_{\phi_I} = \frac{E}{1-\nu^2}\int_{-t/2}^{t/2} (e_\phi^p + \nu e_\theta^p)\,\zeta\, d\zeta \\ M_{\theta_I} = \frac{E}{1-\nu^2}\int_{-t/2}^{t/2} (e_\theta^p + \nu e_\phi^p)\,\zeta\, d\zeta \end{cases} \tag{10}$$

Consider a differential element cut from a shell of revolution by two adjacent meridian planes and two sections perpendicular to the meridian as shown in Figure 1. Let the stress resultants in radial and axial directions be denoted by H and V, respectively. The equilibrium conditions give

$$\begin{cases} (rV)' + \alpha r p_v = 0 \\ (rH)' - \alpha N_\theta + \alpha r p_H = 0 \\ (rM_\phi)' - \alpha M_\theta \cos\phi + \alpha r (H\sin\phi - V\cos\phi) = 0 \end{cases} \tag{11}$$

where p_V and p_H are the components of surface load intensity in the axial and radial directions. The first two of Equation (11) are the conditions of force equilibrium in the axial and radial directions, while the third equation is the condition of moment equilibrium.

Analagous to corresponding Reissner's work in shells with finite deflection but restricted to small strain [15], the system of equations (4), (5), (9) and (11) can be reduced to two simultaneous equations for the unknown meridian angle change β

and a stress function η defined in terms of the horizontal resultant H by

$$\eta = \frac{rH}{Et} \tag{12}$$

The resultant two differential equations are of the following form

$$\begin{cases}
\eta'' + \left[\frac{r_o'}{r_o} - \frac{\alpha'}{\alpha} + \nu\left(\frac{\alpha_o}{r_o} - \frac{\alpha}{r}\right)\cos\phi\right]\eta' \\
\quad - \frac{\alpha}{r}\left[\frac{\alpha_o}{r_o}\cos^2\phi + \nu\left(\frac{r_o'}{r_o}\cos\phi - \frac{r'}{r}\cos\phi - \phi'\sin\phi\right)\right]\eta + \frac{\alpha\alpha_o\sin\phi_o}{r_o}\beta \\
= \frac{\alpha}{r}\left[\frac{\alpha_o}{r_o}\sin\phi\cos\phi + \nu\left(\frac{r_o'}{r_o}\sin\phi - \frac{r'}{r}\sin\phi + \phi'\cos\phi\right)\right]\frac{rV}{Et} \\
\quad - \frac{\alpha}{r_o}\left[\frac{\nu\alpha_o}{r}\cos\phi + \left(\frac{r_o}{r}\right)'\right]\frac{r^2P_H}{Et} - \frac{\alpha}{r}\frac{(r^2P_H)'}{Et} + \frac{\nu\alpha\sin\phi}{r}\frac{(rV)'}{Et} \\
\quad - \frac{\alpha\alpha_o}{r_o}\left[(1-\cos\beta)\cos\phi_o + (\sin\beta - \beta)\sin\phi_o\right] \\
\quad + \frac{\alpha\alpha_o}{r_o}\left[\frac{N\phi_2}{Et}(\cos\phi + \nu\cos\phi_o) - \frac{N\theta_2}{Et}(\cos\phi_o + \nu\cos\phi)\right] - \alpha\left(\frac{N\theta_2'}{Et} - \frac{\nu N\phi_2'}{Et}\right)
\end{cases}$$

$$\begin{cases}
\beta'' + \left(\frac{r'}{r} - \frac{\alpha_o'}{\alpha_o}\right)\beta' - \frac{\alpha}{r}\left(\frac{r'}{r}\cos\phi_o + \nu\phi_o'\sin\phi_o\right)\beta + \nu\left(\frac{\alpha_o\phi'}{\alpha^2} - \frac{\sin\phi_o}{r}\right)\eta'' \\
\quad + \left[\frac{\nu}{\alpha}\phi_o'' + \frac{\nu}{r}(\cos\phi - \cos\phi_o - \nu\cos\phi - \frac{r\alpha_o'}{\alpha\alpha_o})\phi_o' - \frac{\alpha_o r'}{\alpha^2 r}\phi' + \frac{\nu\alpha'}{\alpha}\left(\frac{\sin\phi_o}{r} - \frac{\alpha_o\phi'}{\alpha^2}\right) + \frac{(1+\nu^2)r'}{r^2}\sin\phi_o\right]\eta' \\
\quad + \frac{1}{r}\left[\frac{\alpha_o\sin\phi}{\alpha}\phi'^2 - \phi_o''\cos\phi - \frac{r'}{r}(\cos\phi - \nu\cos\phi - \nu^2\cos\phi_o - \frac{r\alpha_o'}{\alpha\alpha_o})\phi_o'\right. \\
\quad \left. + \frac{1}{r}(\alpha_o\cos^2\phi - \nu^2\alpha\sin\phi_o\sin\phi)\phi' - \frac{\nu(1+\nu)r'^2}{r^2}\sin\phi_o - \frac{12(1-\nu^2)\alpha^2}{t^2}\sin\phi\right]\eta \\
= \frac{1}{r}\left[\frac{\alpha_o\cos\phi}{\alpha}\phi'^2 + \phi_o''\sin\phi + \frac{\alpha\sin\phi}{r}(\cos\phi - \nu\cos\phi - \nu^2\cos\phi_o - \frac{r\alpha_o'}{\alpha\alpha_o})\phi_o'\right. \\
\quad \left. - \frac{\cos\phi}{r}(\alpha_o\sin\phi + \nu^2\alpha\sin\phi_o)\phi' + \frac{\nu(1+\nu)\alpha r'}{r^2}\sin\phi\sin\phi_o - \frac{12(1-\nu^2)\alpha r'}{t^2}\right]\frac{rV}{Et} \\
\quad + \frac{1}{r}\left[\frac{\nu\alpha_o\cos\phi}{r}\phi' - \nu\phi_o'' - \frac{\nu\alpha'}{r}(\cos\phi - \cos\phi_o - \nu\cos\phi - \frac{r\alpha_o'}{\alpha\alpha_o})\phi_o' - \frac{(1+\nu)\alpha r'}{r^2}\sin\phi_o\right]\frac{r^2P_H}{Et} \\
\quad + \frac{\nu\alpha}{r}\left(\frac{\sin\phi_o}{r} - \frac{\alpha_o\phi'}{\alpha^2}\right)\frac{(r^2P_H)'}{Et} + \frac{\sin\phi}{r}\left(\frac{\alpha_o\phi'}{\alpha} - \frac{\nu^2\alpha\sin\phi_o}{r}\right)\frac{(rV)'}{Et} \\
\quad + \frac{\alpha r'}{r^2}\left[(\sin\beta - \beta)\cos\phi_o - (1-\cos\beta)\sin\phi_o\right] + \frac{\nu\alpha\phi_o'}{r}\left[(1-\cos\beta)\cos\phi_o + (\sin\beta - \beta)\sin\phi_o\right] \\
\quad + \left[\phi_o'' + \frac{\alpha'}{r}(\cos\phi - \nu\cos\phi - \nu^2\cos\phi_o - \frac{r\alpha_o'}{\alpha_o\alpha})\phi_o' + \frac{\nu\alpha r'}{r^2}\sin\phi_o\right]\frac{N\theta_2}{Et} \\
\quad - \left[\nu\phi_o'' + \frac{\alpha'\nu}{r}(\cos\phi - \cos\phi_o - \nu\cos\phi - \frac{r\alpha_o'}{\alpha\alpha_o})\phi_o' + \frac{\alpha r'}{r^2}\sin\phi_o\right]\frac{N\theta_2}{Et} \\
\quad + \left(\frac{\alpha_o\phi'}{\alpha} - \frac{\nu^2\alpha\sin\phi_o}{r}\right)\frac{N\theta_2'}{Et} + \nu\alpha\left(\frac{\sin\phi_o}{r} - \frac{\alpha_o\phi'}{\alpha^2}\right)\frac{N\theta_2'}{Et} + \frac{12(1-\nu^2)\alpha}{Et^3}\left[\frac{r'}{r}(M_{\theta_2} - M_{\phi_2}) - M_{\phi_2}'\right]
\end{cases} \tag{13}$$

It should be noted that the inelastic terms, retained in the right-hand side of the equation, are equivalent to an additional set of external loading. In this analysis, no buckling is considered, hence the present analysis is valid only before circumferential buckling occurs.

IV POLYAXIAL STRESS-STRAIN-TIME RELATIONSHIP OF CREEP

To calculate the creep strain, the smooth stress-time curve has often been approximated by a series of finite steps, each of which consists of a constant stress period followed by an instantaneous increment of stress [16]. For applying creep test data under constant stresses to the cases of varying stresses, the mechanical equation of state for uniaxial loading is generalized to [12]

$$\dot{e}^{*p} = F(\sigma^*, e^{*p}) \tag{14}$$

for the multiaxial stress state, where the effective stress σ^* and the effective strain e^{*p} are given as, in the case of the axisymmetric shell,

$$\begin{cases} \sigma^* = \frac{1}{\sqrt{2}}\left[(\sigma_\varphi - \sigma_\theta)^2 + \sigma_\varphi^2 + \sigma_\theta^2\right]^{1/2} \\ e^{*p} = \frac{\sqrt{2}}{3}\left[(e_\varphi^p - e_\theta^p)^2 + (e_\theta^p - e_\zeta^p)^2 + (e_\zeta^p - e_\varphi^p)^2\right]^{1/2} \end{cases} \tag{15}$$

The principal creep strain along the ζ direction has been denoted by e_ζ^p. Since creep strain produces no dilitation,

$$e_\varphi^p + e_\theta^p + e_\zeta^p = 0 \tag{16}$$

Equation (15) reduces to

$$\begin{cases} \sigma^* = (\sigma_\varphi^2 + \sigma_\theta^2 - \sigma_\varphi \sigma_\theta)^{1/2} \\ e^{*p} = \frac{2}{\sqrt{3}}(e_\varphi^{p\,2} + e_\theta^{p\,2} + e_\varphi^p e_\theta^p)^{1/2} \end{cases} \tag{17}$$

in an incremental time interval ΔT, Equation (14) and (17) give

$$[(e_\phi^p+\Delta e_\phi^p)^2+(e_\theta^p+\Delta e_\theta^p)^2+(e_\phi^p+\Delta e_\phi^p)(e_\theta^p+\Delta e_\theta^p)]^{1/2}-(e_\phi^{p2}+e_\theta^{p2}+e_\phi^p e_\theta^p)^{1/2} = \frac{\sqrt{3}}{2}F(\sigma^*, e^{*p})\Delta T \tag{18}$$

The incremental creep strain components, Δe_ϕ^p and Δe_θ^p, are assumed to be proportional to the corresponding deviatoric stress components:

$$\frac{\Delta e_\phi^p}{2\sigma_\phi-\sigma_\theta} = \frac{\Delta e_\theta^p}{2\sigma_\theta-\sigma_\phi} \tag{19}$$

This is commonly assumed in incremental theory of plasticity [17]. With known stresses and creep strains, Equations (18) and (19) give the incremental creep strain components in an incremental time interval ΔT. The total creep strain at any time is the sum of the creep strain increments of all the time steps. From these creep strains, the inelastic terms N_{ϕ_I}, N_{θ_I}, M_{ϕ_I} and M_{θ_I} as given in Equation (10) can be calculated and substituted into Equation (13), to yield a set of equivalent loading.

V NUMERICAL PROCEDURE FOR ANALYZING CORRUGATED TUBE

We now consider a shell with periodic corrugations. Assuming that the corrugations are symmetric about their crests or troughs. One period of the corrugations goes from $z = 0$ to $z = 4c$, so that the wave length is $4c$. Disregarding end effects, the symmetry of the shell meridians suggests that we may consider only half of the period with the following boundary condition:

$$\begin{cases} \beta = 0 \\ \gamma = 0 \end{cases} \qquad \text{at} \qquad z = 0 \ \& \ 2c \tag{20}$$

if we restrict ourself to the problem of corrugated tube subjected to a constant

axial load K, Equation (13) reduces to the following:

$$\begin{cases} \gamma'' + a_1\gamma' + a_2\gamma + a_3\beta = g_1 \\ \beta'' + a_4\beta' + a_5\beta + a_6\gamma'' + a_7\gamma' + a_8\gamma = g_2 \end{cases} \tag{21}$$

where

$$\begin{aligned}
a_1 &= \frac{r_0'}{r_0} - \frac{\alpha'}{\alpha} + \nu\left(\frac{\alpha_0}{r_0} - \frac{\alpha}{r}\right)\cos\phi \\
a_2 &= -\frac{\alpha}{r}\left[\frac{\alpha_0}{r_0}\cos^2\phi + \nu\left(\frac{r_0'}{r_0}\cos\phi - \frac{r'}{r}\cos\phi - \phi'\sin\phi\right)\right] \\
a_3 &= \frac{\alpha\alpha_0}{r_0}\sin\phi_0 \\
a_4 &= \frac{r'}{r} - \frac{\alpha_0'}{\alpha_0} \\
a_5 &= -\frac{\alpha}{r}\left(\frac{r'}{r}\cos\phi_0 + \nu\phi_0'\sin\phi_0\right) \\
a_6 &= \nu\left(\frac{\alpha_0\phi'}{\alpha^2} - \frac{\sin\phi_0}{r}\right) \\
a_7 &= \frac{\nu}{\alpha}\phi_0'' + \frac{\nu}{r}\left(\cos\phi - \cos\phi_0 - \nu\cos\phi - \frac{r\alpha_0'}{\alpha\alpha_0}\right)\phi_0' - \frac{\alpha_0 r'}{\alpha^2 r}\phi' + \frac{\nu\alpha'}{\alpha}\left(\frac{\sin\phi_0}{r} - \frac{\alpha_0\phi'}{\alpha^2}\right) + \frac{(1+\nu^2)r'}{r^2}\sin\phi_0 \\
a_8 &= \frac{1}{r}\left[\frac{\alpha_0\sin\phi}{\alpha}\phi'^2 - \phi_0''\cos\phi - \frac{r'}{r}\left(\cos\phi - \nu\cos\phi - \nu^2\cos\phi_0 - \frac{r\alpha_0'}{\alpha\alpha_0}\right)\phi_0'\right. \\
&\qquad \left. + \frac{1}{r}\left(\alpha_0\cos^2\phi - \nu^2\alpha\sin\phi_0\sin\phi\right)\phi' - \frac{\nu(1+\nu)r'^2}{r^2}\sin\phi_0 - \frac{12(1-\nu^2)\alpha^2}{t^2}\sin\phi\right] \\
g_1 &= \frac{\alpha}{r}\left[\frac{\alpha_0}{r_0}\sin\phi\cos\phi + \nu\left(\frac{r_0'}{r_0}\sin\phi - \frac{r'}{r}\sin\phi + \phi'\cos\phi\right)\right]\frac{K}{2\pi Et} \\
&\quad - \frac{\alpha\alpha_0}{r_0}\left[(1-\cos\beta)\cos\phi_0 + (\sin\beta - \beta)\sin\phi_0\right] \\
&\quad + \frac{\alpha\alpha_0}{r_0}\left[\frac{N_{\theta_2}}{Et}(\cos\phi + \nu\cos\phi_0) - \frac{N_{\phi_2}}{Et}(\cos\phi_0 + \nu\cos\phi)\right] - \alpha\left(\frac{N_{\theta_2}'}{Et} - \nu\frac{N_{\phi_2}'}{Et}\right) \\
g_2 &= \frac{1}{r}\left[\frac{\alpha_0\cos\phi}{\alpha}\phi'^2 + \phi_0''\sin\phi + \frac{\alpha\sin\phi}{r}\left(\cos\phi - \nu\cos\phi - \nu^2\cos\phi_0 - \frac{r\alpha_0'}{\alpha\alpha_0}\right)\phi_0'\right. \\
&\qquad \left. - \frac{\cos\phi}{r}\left(\alpha_0\sin\phi + \nu^2\alpha\sin\phi_0\right)\phi' + \frac{\nu(1-\nu)\alpha r'}{r^2}\sin\phi\sin\phi_0 - \frac{12(1-\nu^2)\alpha r'}{t^2}\right]\frac{K}{2\pi Et} \\
&\quad + \frac{\alpha r'}{r^2}\left[(\sin\beta - \beta)\cos\phi_0 - (1-\cos\beta)\sin\phi_0\right] + \frac{\nu\alpha\phi_0'}{r}\left[(1-\cos\beta)\cos\phi_0 + (\sin\beta - \beta)\sin\phi_0\right] \\
&\quad + \left[\phi_0'' + \frac{\alpha}{r}\left(\cos\phi - \nu\cos\phi - \nu^2\cos\phi_0 - \frac{r\alpha_0'}{\alpha\alpha_0}\right)\phi_0' + \frac{\nu\alpha r'}{r^2}\sin\phi_0\right]\frac{N_{\phi_2}}{Et} \\
&\quad - \left[\nu\phi_0'' + \frac{\nu\alpha}{r}\left(\cos\phi - \cos\phi_0 - \nu\cos\phi - \frac{r\alpha_0'}{\alpha\alpha_0}\right)\phi_0' + \frac{\alpha r'}{r^2}\sin\phi_0\right]\frac{N_{\theta_2}}{Et} \\
&\quad + \left(\frac{\alpha_0\phi'}{\alpha} - \frac{\nu^2\alpha\sin\phi_0}{r}\right)\frac{N_{\phi_2}'}{Et} + \nu\alpha\left(\frac{\sin\phi_0}{r} - \frac{\alpha_0\phi'}{\alpha^2}\right)\frac{N_{\theta_2}'}{Et} + \frac{12(1-\nu^2)\alpha}{Et^3}\left[\frac{r'}{r}(M_{\theta_2} - M_{\phi_2}) - M_{\phi_2}'\right]
\end{aligned} \tag{22}$$

Equation (21) is solved by finite difference and iterative technique as shown in the following.

On the basis of conventional central difference formulae

$$\begin{cases} \left(\frac{dy}{d\xi}\right)_n = \frac{y_{n+1}-y_n}{2h_{n+1}} + \frac{y_n-y_{n-1}}{2h_n} \\ \left(\frac{d^2y}{d\xi^2}\right)_n = \frac{2}{h_n+h_{n+1}}\left(\frac{y_{n+1}-y_n}{2h_{n+1}} - \frac{y_n-y_{n-1}}{2h_n}\right) \end{cases} \qquad (23)$$

where

$$h_n = \xi_n - \xi_{n-1}$$

the differential Equation (21) can be written in finite difference form at any stations n except at z=o and 2c,

$$\begin{cases} A_1^n \gamma_{n+1} + A_2^n \gamma_n + A_3^n \gamma_{n-1} + a_3^n \beta_n = g_1^n \\ A_4^n \beta_{n+1} + A_5^n \beta_n + A_6^n \beta_{n-1} + A_7^n \gamma_{n+1} + A_8^n \gamma_n + A_9^n \gamma_{n-1} = g_2^n \end{cases} \qquad (24)$$

where

$$
\begin{cases}
A_1^n = \frac{1}{\ell_{n+1}}\left(\frac{2}{\ell_n+\ell_{n+1}} + \frac{a_1^n}{2}\right) \\
A_2^n = \frac{1}{\ell_n \ell_{n+1}}\left[\frac{a_1^n}{2}(\ell_{n+1}-\ell_n) - 2\right] + a_2^n \\
A_3^n = \frac{1}{\ell_n}\left(\frac{2}{\ell_n+\ell_{n+1}} - \frac{a_1^n}{2}\right) \\
A_4^n = \frac{1}{\ell_{n+1}}\left(\frac{2}{\ell_n+\ell_{n+1}} + \frac{a_4^n}{2}\right) \\
A_5^n = \frac{1}{\ell_n \ell_{n+1}}\left[\frac{a_4^n}{2}(\ell_{n+1}-\ell_n) - 2\right] + a_5^n \\
A_6^n = \frac{1}{\ell_n}\left(\frac{2}{\ell_n+\ell_{n+1}} - \frac{a_4^n}{2}\right) \\
A_7^n = \frac{1}{\ell_{n+1}}\left(\frac{2a_5^n}{\ell_n+\ell_{n+1}} + \frac{a_7^n}{2}\right) \\
A_8^n = \frac{1}{\ell_n \ell_{n+1}}\left[\frac{a_7^n}{2}(\ell_{n+1}-\ell_n) - 2a_6^n\right] + a_8^n \\
A_9^n = \frac{1}{\ell_n}\left(\frac{2a_6^n}{\ell_n+\ell_{n+1}} - \frac{a_7^n}{2}\right)
\end{cases}
\qquad (25)
$$

The superscript n denotes the value at the n^{th} station. By eliminating β's, Equation (24) yields:

$$B_1^n \eta_{n+2} + B_2^n \eta_{n+1} + B_3^n \eta_n + B_4^n \eta_{n-1} + B_5^n \eta_{n-2} = G^n \qquad (26)$$

and

$$\beta_n = \frac{1}{a_3^n}\left(g_1^n - A_1^n \eta_{n+1} - A_2^n \eta_n - A_3^n \eta_{n-1}\right) \qquad (27)$$

where

$$
\begin{cases}
B_1^n = -\dfrac{A_2^n A_1^{n+1}}{a_3^{n+1}} \\
B_2^n = -\dfrac{A_4^n A_3^{n+1}}{a_3^{n+1}} - \dfrac{A_5^n A_1^n}{a_3^n} + A_7^n \\
B_3^n = -\dfrac{A_4^n A_3^{n+1}}{a_3^{n+1}} - \dfrac{A_5^n A_3^n}{a_3^n} - \dfrac{A_6^n A_1^{n-1}}{a_3^{n-1}} + A_8^n \\
B_4^n = -\dfrac{A_5^n A_2^{n-1}}{a_3^{n-1}} - \dfrac{A_5^n A_3^n}{a_3^n} + A_9^n \\
B_5^n = -\dfrac{A_6^n A_3^{n-1}}{a_3^{n-1}} \\
G^n = g_2^n - \dfrac{A_4^n}{a_3^{n+1}} g_1^{n+1} - \dfrac{A_5^n}{a_3^n} g_1^n - \dfrac{A_6^n}{a_3^{n-1}} g_1^{n-1}
\end{cases}
\qquad (28)
$$

The set of equations, Equation (26), will be solved by the procedure equivalent to solution by the method of Gaussian elimination used in other problems of shells of revolution [18,19]. The elimination technique proceeds as follows: Let the two points z=o, 2c be denoted by n=o and n=N respectively, so that

$$
\begin{cases}
\beta_o = \beta_N = 0 \\
\gamma_o = \gamma_N = 0
\end{cases}
\qquad (29)
$$

From symmetry, we also have

$$
\begin{cases}
\beta_{-1} = -\beta_1 \quad ; \quad \beta_{N+1} = -\beta_{N-1} \\
\gamma_{-1} = -\gamma_1 \quad ; \quad \gamma_{N+1} = -\gamma_{N-1}
\end{cases}
\qquad (30)
$$

The first of Equation (26) i.e. n=1 is solved for γ_1 in terms γ_2 and γ_3 :

$$\eta_1 = \frac{1}{B_3' - B_5'} \left(G' - B_2' \eta_2 - B_1' \eta_3 \right) \qquad (31)$$

This result is substituted into the next equation n=2 and η_2 will be found in terms of η_3 and η_4, and so on. Finally the last equation of Equation (26) will determine η_{N-1}, and then with $\eta_N = 0$, all of the η's will be calculated in reverse order. Accordingly, we may write η_n as

$$\eta_n = R_n - P_n \eta_{n+1} - Q_n \eta_{n+2} \qquad (32)$$

From Equations (29) through (32), we have

$$\begin{cases} R_1 = \dfrac{G'}{B_3' - B_5'} \; ; & R_0 = 0 \\ P_1 = \dfrac{B_2'}{B_3' - B_5'} \; ; & P_0 = 0 \\ Q_1 = \dfrac{B_1'}{B_3' - B_5'} \; ; & Q_0 = 0 \end{cases} \qquad (33)$$

Substitution of Equation (32) into Equation (26) yields the result:

$$\begin{cases} R_n = \dfrac{1}{D_n} \left[G^n - B_4^n R_{n-1} - B_5^n \left(R_{n-2} - P_{n-2} R_{n-1} \right) \right] \\ P_n = \dfrac{1}{D_n} \left(B_2^n - B_4^n Q_{n-1} + B_5^n P_{n-2} Q_{n-1} \right) \\ Q_n = \dfrac{B_1^n}{D_n} \end{cases} \qquad (34)$$

$n = 2, \cdots, N-2$

where

$$D_n = B_3^n - B_4^n P_{n-1} + B_5^n \left(P_{n-1} P_{n-2} - Q_{n-2} \right)$$

This recurrance relation together with the initial values from Equation (33) give

all the R_n's, P_n's and Q_n's up to R_{n-2}, P_{n-2} and Q_{n-2}. The last of Equation (26), n=N-1, and symmetry condition, Equation (30), determine γ_{N-1} as

$$\gamma_{N-1} = \frac{R_{N-1}}{1-Q_{N-1}} \tag{35}$$

where R_{n-1} and Q_{n-1} are the extension of Equation (34) to n=N-1. With γ_N and γ_{N-1} known, γ_{N-2}, γ_{N-3}, $\cdots$, γ_2, γ_1 can be found from Equation (32) and then all the β's can readily be obtained from Equation (27). This process is readily programmed for the high speed digital computer.

The stress resultants, meridian strains and displacements defined in accordance with Figure 1 are obtained from β and γ, as follows

$$\left\{\begin{aligned}
N_\varphi &= \frac{1}{r}\left(\gamma\cos\phi + \frac{K}{2\pi}\sin\phi\right) \\
N_\theta &= \frac{1}{\alpha}\gamma' \\
Q &= \frac{1}{r}\left(-\gamma\sin\phi + \frac{K}{2\pi}\cos\phi\right) \\
e_{\varphi_m} &= \frac{1}{Et}\left[N_\varphi + N_{\varphi_I} - \nu(N_\theta + N_{\theta_I})\right] \\
e_{\theta_m} &= \frac{1}{Et}\left[N_\theta + N_{\theta_I} - \nu(N_\varphi + N_{\varphi_I})\right] \\
\alpha &= \alpha_0(1+e_{\varphi_m}) \\
u &= r_0 e_{\theta_m} \\
w &= \int \alpha_0\left[(1+e_{\varphi_m})\sin\phi - \sin\phi_0\right] d\xi
\end{aligned}\right. \tag{36}$$

In the inelastic problem, the loading path is important. The time is increased in increments in the case of creep deformation. In each step of time increment, the initial values of r, Φ, e_φ^p and e_θ^p at each

station are known. The stresses σ_φ, σ_ϑ, σ^* and the strains e_φ, e_ϑ, e^{*p} can be calculated from Equations (4), (7), (8) and (17). The incremental creep strains Δe_φ^p and Δe_ϑ^p in an incremental time interval ΔT are obtained from Equations (18) and (19) with given function $F(\sigma^*, e^{*p})$. Inelastic stress resultants and sectional moments are found from Equation (10). With assumed values of β and γ, the coefficients a_i's and A_i's can be calculated. Equation (24) can then be solved for new values of β and γ. The procedure is repeated until the differences between the successive β's and γ's are within desired tolerances. The calculation can then be extended to the next time increment. In the following numerical example, the tolerance for η of 0.01%, was used.

VI NUMERICAL EXAMPLES

The above procedure is first applied to the static deformation of a corrugated tube similar to the one tested by Donnell [20]. The meridian consists of circular arcs. The dimensions (Figure 2) are

$$\begin{cases} a = 5.33 \text{ in} \\ b = 0.235 \text{ in} \\ c = 0.670 \text{ in} \\ t = 0.065 \text{ in} \end{cases}$$

and $E = 30 \times 10^6$ psi, $\nu = 0.3$. Figure 3 shows the axial load deflection curve for tensile and compressive loadings. The linear solution checks very well with that of Clark and Reissner [21]. It is seen that the corrugated tube under tensile axial force is stiffer than under compressive axial force. This was pointed out by Hamada [22], in the elastic large deflection theory of shell of revolution.

The incremental procedure is also applied to a 7075-T6 aluminum alloy

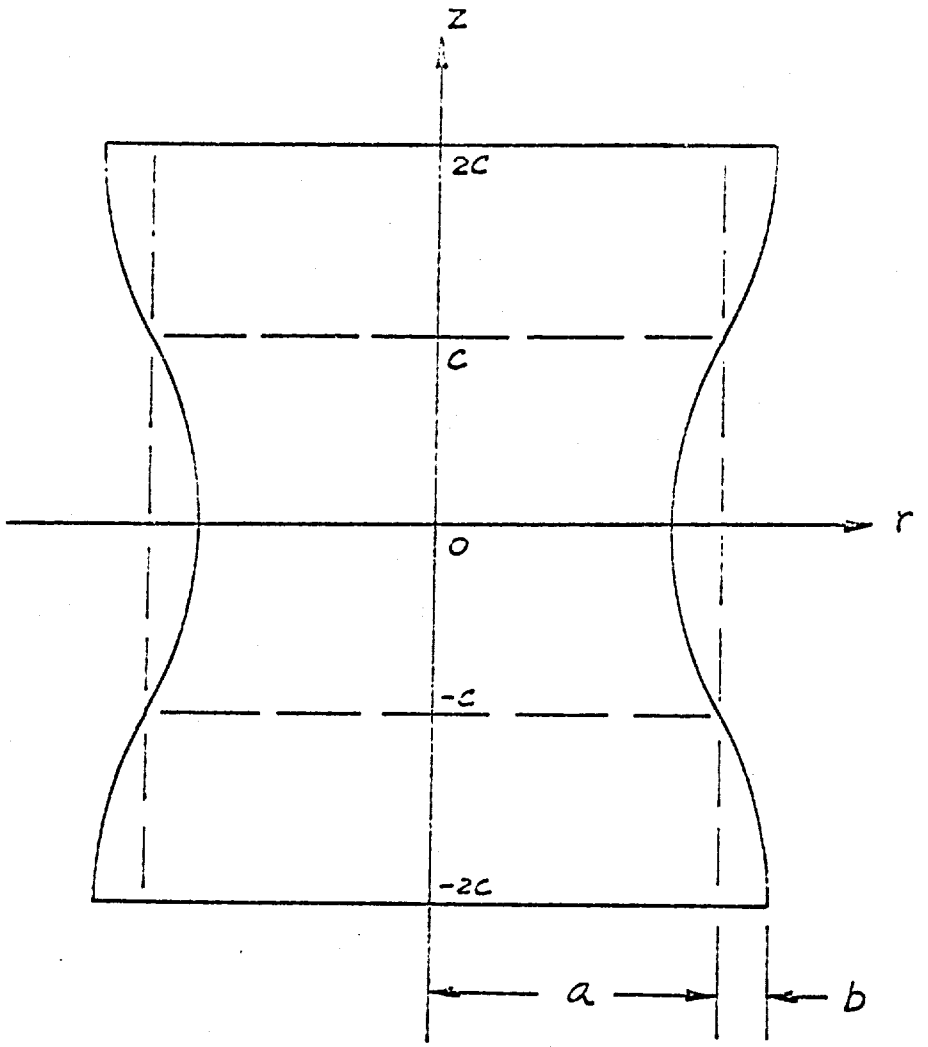

Figure 2. Circular Arc Corrugation

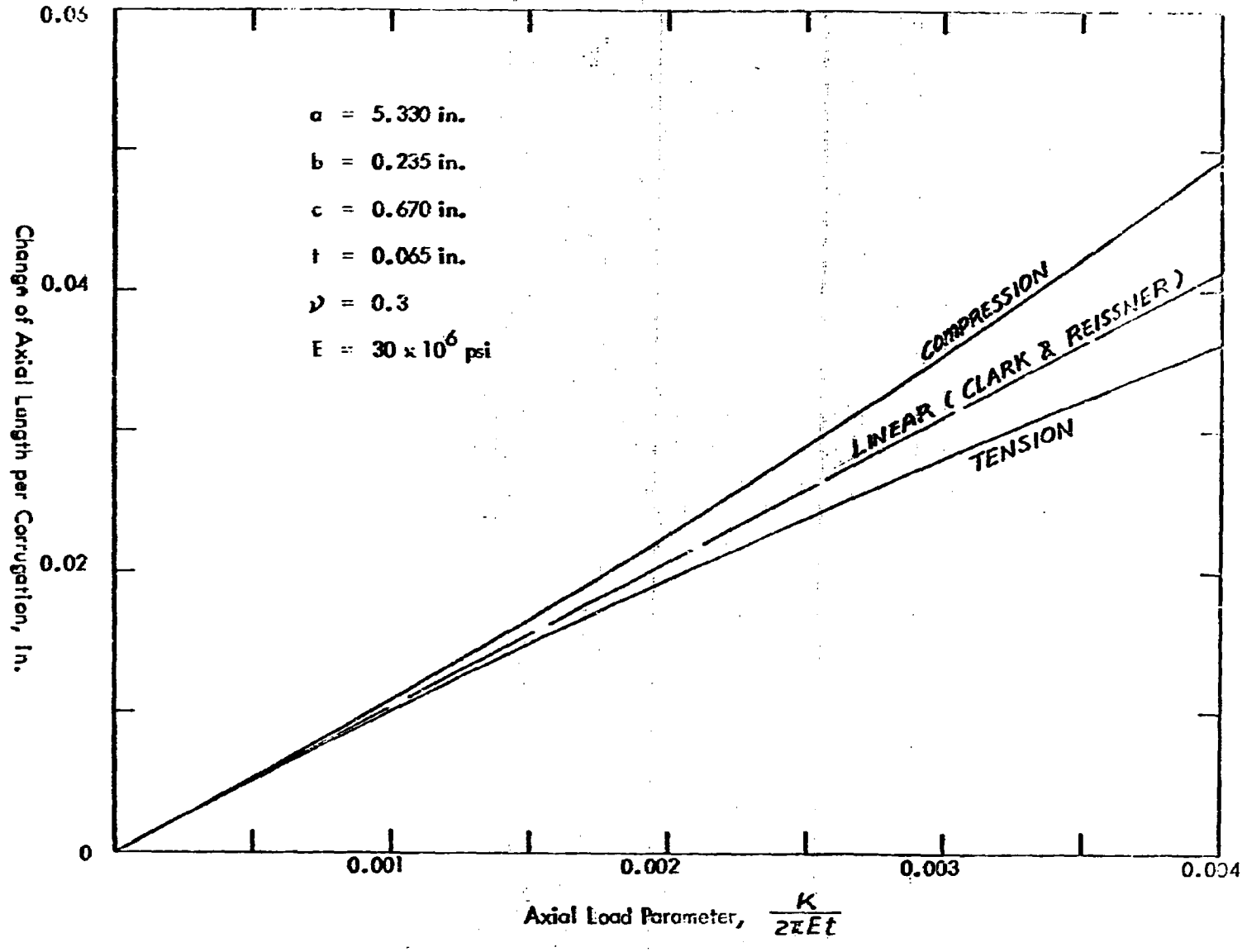

Figure 3. Load Deflection Curve of a Corrugated Tube

corrugated tube undergoing large deformation at 600° F. The geometric dimensions are same as above. The applied axial load is 2124 lbs. The uniaxial creep characteristics of the material are approximated by the following stress-strain-time-relation:

$$\epsilon = \frac{\sigma}{E} + A T^{k} \sinh (B\sigma)$$

where

$A = 5.25 \times 10^{-7}$/hr

$B = 1.92 \times 10^{-3}$ in^2/lb

$k = 0.66$

$E = 5.2 \times 10^{6}$ psi

ϵ = total strain

σ = stress in psi

T = time in hour

and Poisson's ratio ν is 0.32. The creep characteristics are assumed to be the same in tension and in compression. The first time increment was taken to be 0.0001 hr. The subsequent time increment was increased in each step at constant rate. There were 100 time increments to reach the total of 16.66 hours. The 100th time increment was .5050 hr. The number of finite difference stations along the midsurface in half period of corrugation was 49. The number of grid points across the thickness was 13. The tolerance used in the present calculation was 0.01% for η . To obtain this degree of accuracy, 3 cycles of iteration was generally found to be sufficient. The computation was carried out on an IBM 360 and the computing time for this creep analysis was within one minute. Figure 4 shows the increase of total axial deflection with time. The variations of the extreme fiber stresses at two ends at different instants are shown in Figures 5 and 6.

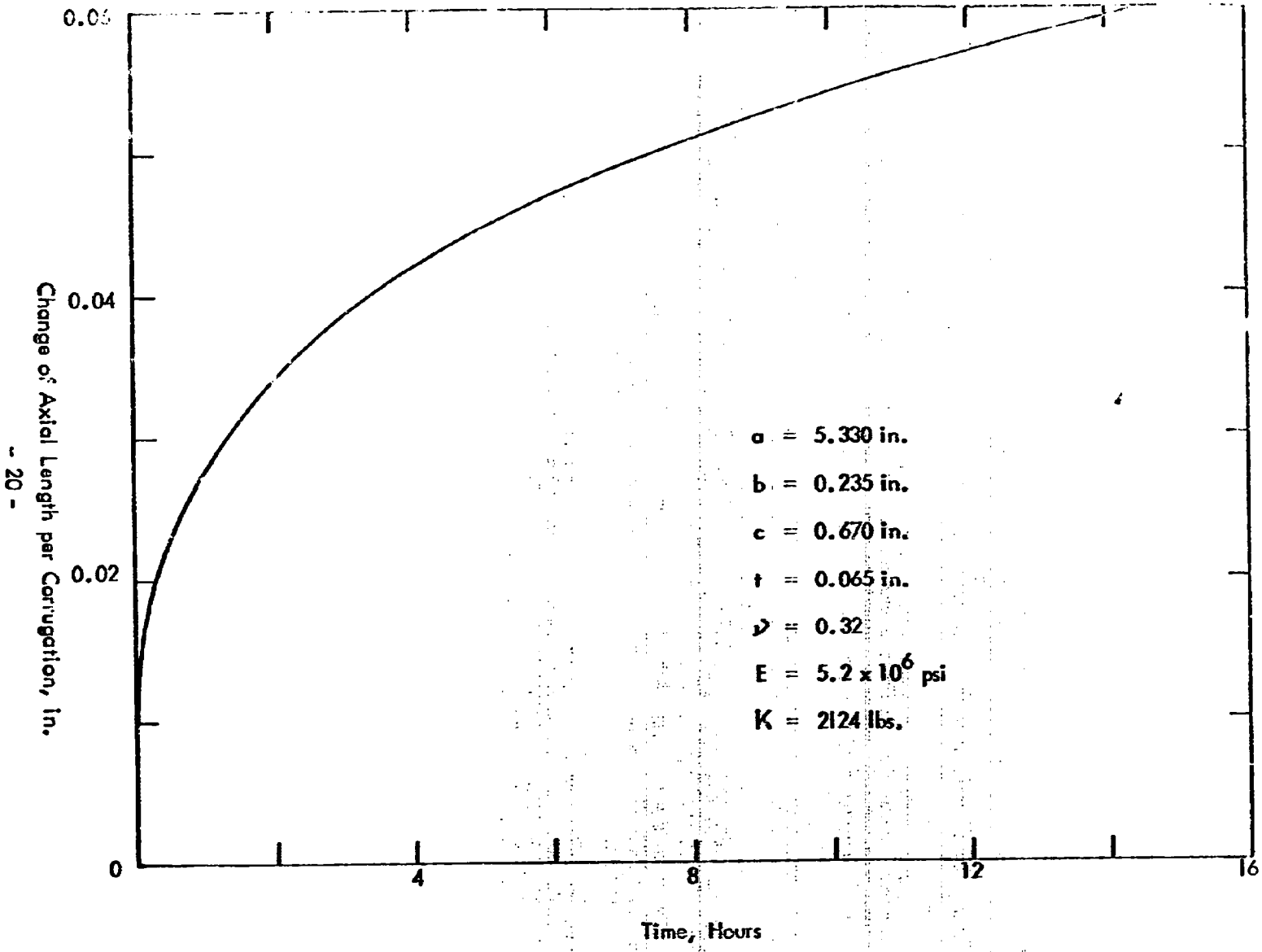

Figure 4. Variation of Axial Elongation with Time

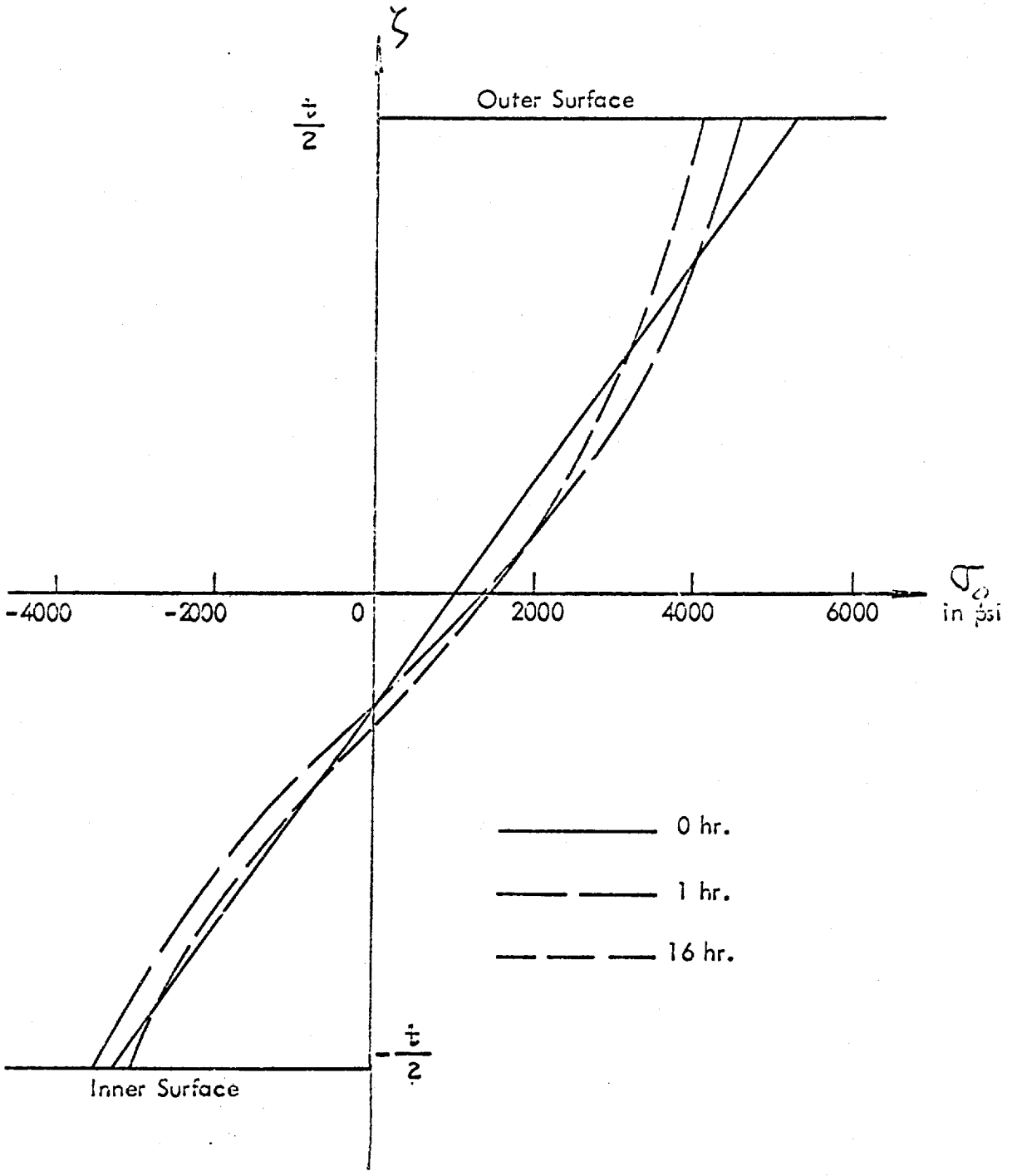

Figure 5. Variation of Longitudinal Stress Across The Thickness at Section z=o at Different Instants of Time

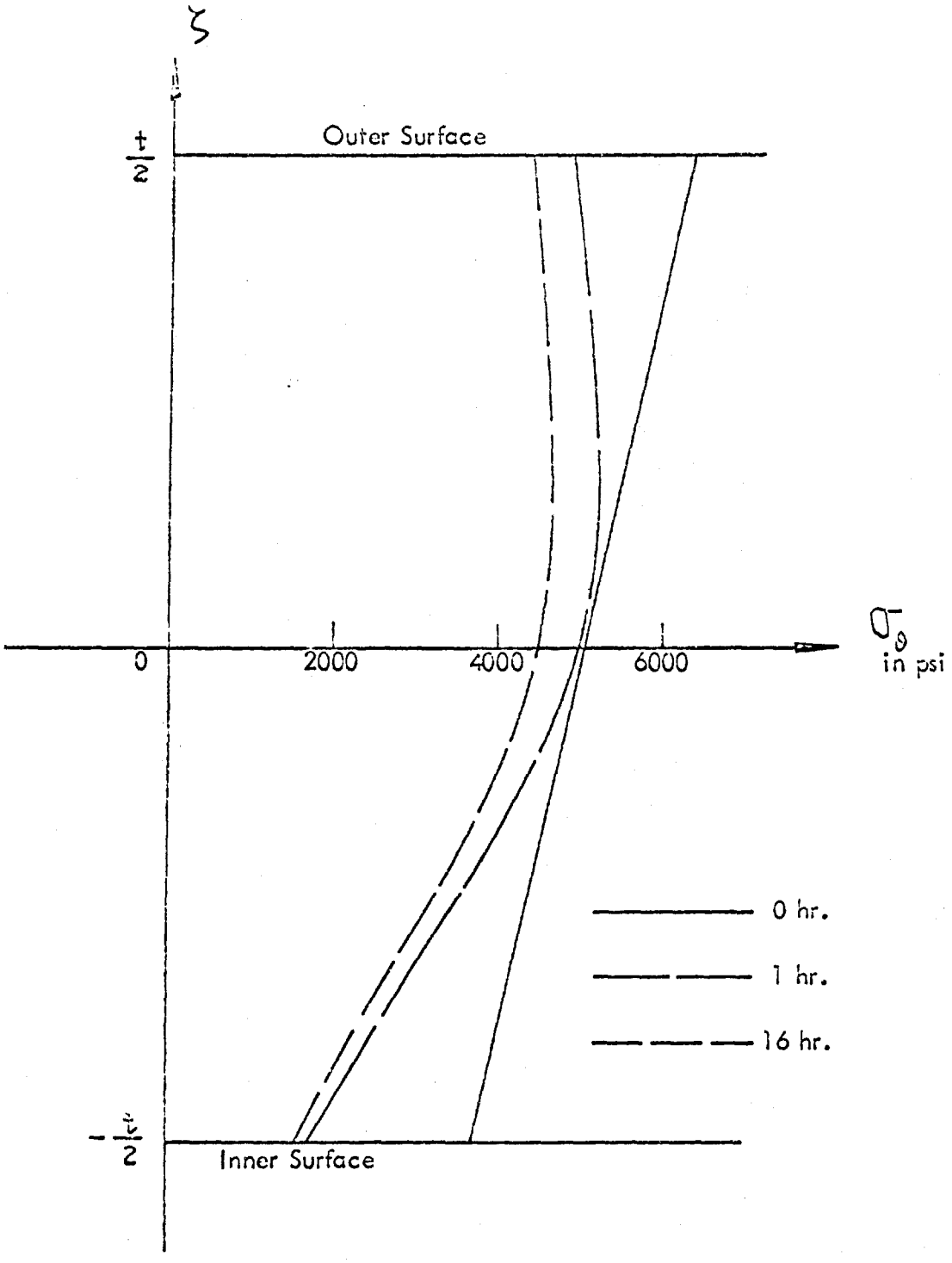

Figure 6. Variation of Circumferential Stress Across the Thickness at Section z=o at Different Instants of Time

VII CONCLUSIONS

A numerical method is shown for the creep analysis of axisymmetric shells subject to axisymmetric loadings with large deflections. A numerical example of creep deformation of a corrugated tube under an axial load with finite deflection is given. Vertical displacement and stress distributions of the tube at different instants of time after loading are shown. This method may be extended to analyzing elastic-plastic deformation of shells of revolution with finite deflection.

In the numerical example of creep analysis, 100 time increments were used. The time increment increases from an initial value of 0.0001 hr. to 0.5050 hr. for the 100th increment. The convergence of the solution with the number of finite difference stations along the meridian was found to be good. It was found that the use of 25 and 49 finite difference stations gave only 0.2% difference in total axial deflection. The number of grids across the thickness and time increments used also provided good convergence.

Part B

Effect of the Secondary Slip System on Early Fatigue Damage

I SUMMARY

A face-centered-cubic polycrystal under cyclic loading is considered. It is shown that slip in the primary slip system causes the resolved shear stress in a second slip system to increase to the critical value and then this second slip system slides. Slip in this second slip system greatly increases the rate of the local plastic strain build-up in the primary slip system. Hence the occurrence of the second active slip system may greatly increase rate of extrusion and intrusion commonly observed in face-centered-cubic metals.

I INTRODUCTION

Fatigue failure is characterized by fracture under repeated stress far below the static fracture strength and usually occurs by the processes of crack nucleation, propagation and final rupture. Even though regions near the nucleus of the crack and along its path of propagation may be highly distorted, material away from these regions may not show any significant macroscopic plastic deformation. In a single crystal, the fatigue crack often lies along a slip plane. Ewing and Humphrey [23], studied the formation of cracks by the microscopic observations of the surface appearance of specimens. Their tests on Swedish iron revealed that very few slip lines were produced by the first few thousand cycles but as the test progressed, more slip lines formed. These slip lines are the intersections of sliding planes with the free surface. As stressing continues, bands of slip are produced and intensified. Slip lines in fatigue specimens were found to be spaced not as evenly as those in unidirectional loading. Fatigue cracks eventually are formed in these intense slip bands.

The first quantitative physical theory of fatigue crack nucleation based on the microstress field caused by slip was proposed by Lin and Ito [24, 25]. The theory was applied to study the influence of strain-hardening, grain size and mean stress on early fatigue damage [26, 27]. The results show that the increase of the strain-hardening rate and/or the decrease of the grain size decreases the rate of early fatigue damage, and the effect of mean stress on the number of cycles to failure was found to lie between the values predicted by Gerber's parabola and by the modified Goodman's line.

The Lin-Ito theory was in part based on the experimentally observed formation of slip bands and is briefly reviewed here for reference. The slip lines formed in forward loading and those formed in reverse loading are very closely

spaced but distinct from each other and occur in the same slip band. Positive slip occurs in one slip line in forward loading and negative slip occurs in a nearby slip line in reverse loading. Since lattice imperfections exist in all metals, initial heterogeneous microstress fields exist in all metals. The initial stress field favorable to this type of slip formation is clearly one producing resolved shear stresses of opposite sign in two closely spaced, parallel thin slices. As shown in Figure 7, two thin slices in a most-favorably-oriented crystal located at the free surface have an initial resolved shear stress field which is positive in slice P and negative in slice Q . Under tensile loading, the positive critical shear stress is attained and hence slip occurs in P . Since the residual stress field caused by slip is continuous, slip in P relieves the positive resolved shear stress not only in P but also in Q . This helps to keep Q from reaching the positive critical shear stress in tensile loading, and also increases the negative resolved shear stress that causes Q to slide more easily in reverse loading. When the negative resolved shear stress in Q reaches the critical shear stress in reverse loading, slip occurs in Q and a new residual stress field is produced. The new stress field increases the positive resolved shear stress not only in Q but also in P . This increase of positive resolved shear stress in P causes P to slide more easily in the next tensile loading. This process is repeated for every cycle and builds up the local plastic strain at these two thin slices, P and Q . The plastic strain in P and Q tends to push out the region between them and starts an extrusion. If the signs of initial stress in P and Q are changed, an intrusion instead of extrusion will be initiated. Thus, the continuity of the relief of stress provides a natural gating mechanism for the monotonic build-up of local plastic strain and no special gating mechanism, such as a specific movement of the Lomer-Cottrell barrier, as proposed by Kennedy [28] is necessary.

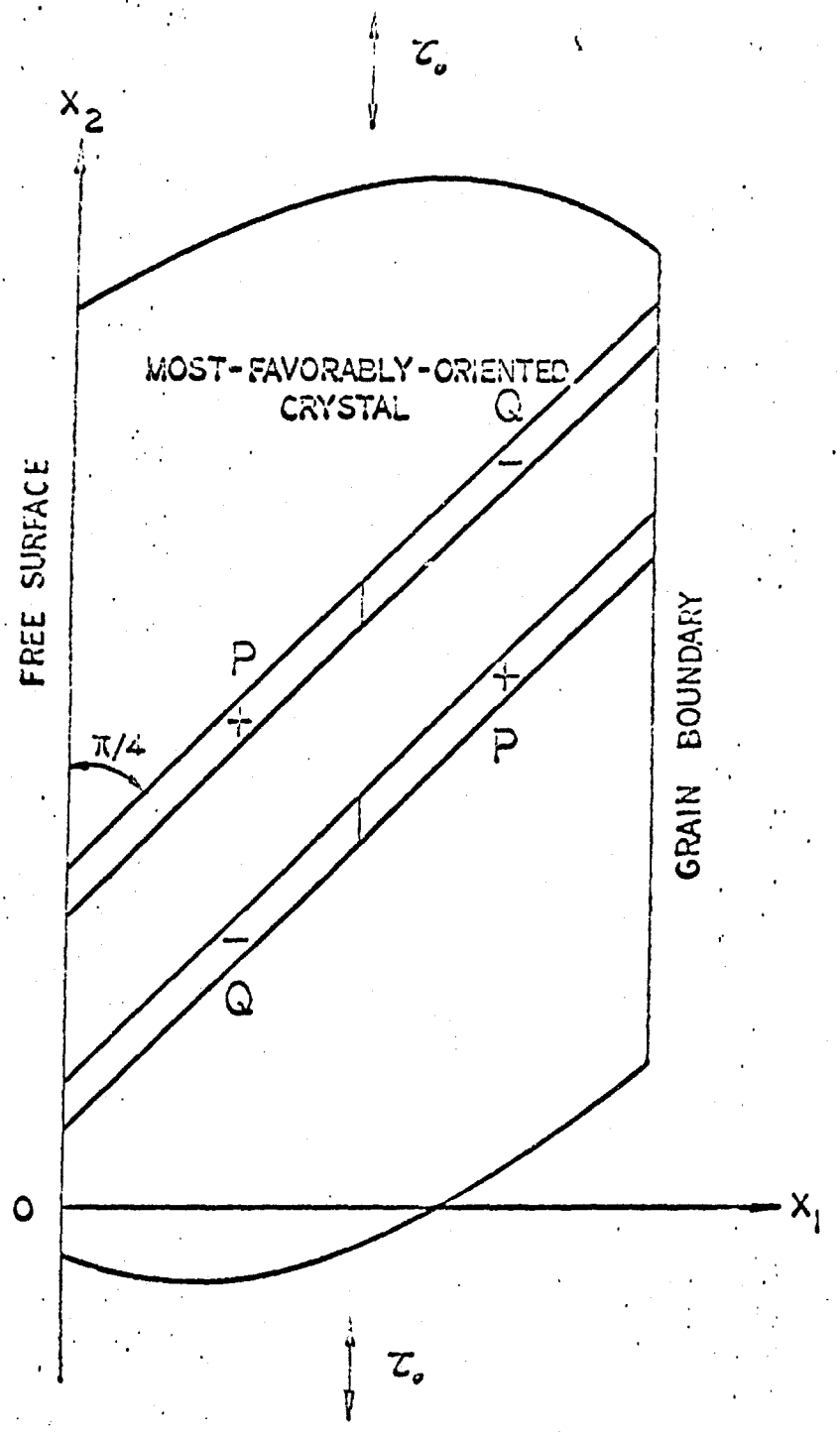

Figure 7. Lin-Ito Fatigue Model

In Lin and Ito's calculation, it was assumed that only the most-favorably-oriented slip system would be activated. This system is referred to as the primary slip system. For face-centered-cubic (fcc) metals such as aluminum and its alloys, each crystal has four slip planes with three slip directions on each plane and hence there are twelve slip systems. During the process of extrusion, the material is elongated along the direction of the extrusion and hence a tensile stress is developed in the region between P and Q. Similarly, a compressive stress is developed along the direction of an intrusion. This stress will cause other slip systems to slide. The purpose of the present study is to evaluate the slip in these secondary slip systems during the early stages of fatigue.

III RESOLVED SHEAR STRESS FIELD CAUSED BY SLIP

Among the different mechanisms of plastic deformation in metals, crystallographic slip has been shown to be the principal process of plastic deformation in face-centered-cubic metals at low and intermediate temperatures [29]. From single-crystal tests, it has been shown [30, 31] that slip depends on the resolved shear stress and is independent of the normal stress on the slip plane. The resolved shear stress necessary to initiate or to cause further slip is generally known as the critical shear stress. Those slip systems in the crystal with highest resolved shear stress are called the most-favorably-oriented slip systems and are the first to reach the critical shear stress. When the critical shear stress is reached in some region in the most-favorably-oriented crystal in the body, slip occurs and causes plastic strain. Should the load be removed after sliding in the region, the slip would remain and cause a residual stress field. If the load is applied again, assuming no further slip during this reloading, the residual stress plus the applied aggregate stress, gives the resultant stress field in the body. To find the residual stress due to localized

slip, the analogy between the plastic strain gradient and a body force in causing stresses in an elastic medium first shown by Reissner [32] and developed by Eshelby [33] and Lin [12] is used. Referring to a set of rectangular axes, let the plastic strain tensor due to slip be denoted by e''_{ij}. The strain distribution in a body with plastic strain under external load is the same as that in a purely elastic body with the additional equivalent body force and surface traction:

$$\begin{cases} \bar{F}_i = -2\mu e''_{ij,j} \\ \overset{\nu}{\bar{T}}_i = 2\mu e''_{ij}\nu_j \end{cases} \tag{1}$$

where μ is the shear modulus, ν_i is the component of the unit surface normal ν on x_i axis, and subscript after a comma denotes differentiation with respect to a coordinate variable. The residual stress field of the actual body will be given as:

$$\tau_{ij_r} = \tau_{ij_s} - 2\mu e''_{ij} \tag{2}$$

where τ_{ij_s} is the stress field caused by $\bar{F}_i$ and $\overset{\nu}{\bar{T}}_i$.

The aggregate considered is of fine grain; grain size being small compared with the total volume of the aggregate. On Figure 7, x_1, x_2 and x_3 are a set of orthogonal cartesian coordinates, where the x_3 axis is parallel to the width of slices P and Q, and x_1 axis is normal to the free surface. Since the two slices P and Q are parallel and the thickness of each slice is much less than its width, the deformation state can be considered under plane strain. By using Airy's stress function, the stress distribution caused by a point force in a semi-infinite plate for plane stress has been given by Melan [34]. Melan's solution was modified for plane strain by Tung and Lin [35]. This stress function is used in the calculation of slip strains and stresses in polycrystalline aggregates near the

free surface. Let $\tau_{ij}^{k}(x,\bar{x})$ be the stress at $x \equiv (x_1, x_2)$ due to a unit force acting at $\bar{x} \equiv (\bar{x}_1, \bar{x}_2)$ along the direction of x_k axis, and $\phi_k(x,\bar{x})$ be the corresponding stress function; we have:

$$\begin{cases} \tau_{11}^{k}(x,\bar{x}) = \dfrac{\partial^2 \phi_k}{\partial x_2^2} \\ \tau_{22}^{k}(x,\bar{x}) = \dfrac{\partial^2 \phi_k}{\partial x_1^2} \\ \tau_{12}^{k}(x,\bar{x}) = -\dfrac{\partial^2 \phi_k}{\partial x_1 \partial x_2} \end{cases} \qquad k = 1, 2 \tag{3}$$

where the stress functions are given as

$$\begin{cases} \phi_1(x,\bar{x}) = -(\rho+q)(x_2-\bar{x}_2)(\theta_1+\theta_2) + \dfrac{q_0}{2}(x_1-\bar{x}_1)\log\dfrac{\Sigma_1}{\Sigma_2} + 2\rho\dfrac{x_1\bar{x}_1(x_1+\bar{x}_1)}{\Sigma_2} \\ \phi_2(x,\bar{x}) = (\rho+q)(x_1-\bar{x}_1)(\theta_1+\theta_2) + \dfrac{q_0}{2}(x_2-\bar{x}_2)\log\dfrac{\Sigma_1}{\Sigma_2} - 2\rho\dfrac{x_1\bar{x}_1(x_2-\bar{x}_2)}{\Sigma_2} \end{cases} \tag{4}$$

and

$$\begin{cases} \rho = \dfrac{1}{4\pi(1-\sigma)} \\ q_0 = \rho(1-2\sigma) \\ \theta_1 = \tan^{-1}\dfrac{x_2-\bar{x}_2}{x_1-\bar{x}_1} \qquad -\pi \le \theta_1 < \pi \\ \theta_2 = \tan^{-1}\dfrac{x_2-\bar{x}_2}{x_1+\bar{x}_1} \qquad -\dfrac{\pi}{2} \le \theta_2 < \dfrac{\pi}{2} \\ \Sigma_1 = (x_1-\bar{x}_1)^2 + (x_2-\bar{x}_2)^2 \\ \Sigma_2 = (x_1+\bar{x}_1)^2 + (x_2-\bar{x}_2)^2 \end{cases} \tag{5}$$

It should be pointed out that Equations (3) and (4) are valid only when $x \neq \bar{x}$.

Consider a point $\bar{x}$ in a crystal that has slid. Let $\xi(m)$ be normal to the slip plane and $\eta(m)$ be in the sliding direction of the m^{th} active slip system at the source point $\bar{x}$, and $e''(\bar{x}, m)$ be the plastic shear strain caused by this slip. This plastic strain, referring to x_i-coordinates, is then

$$e_{ij}''(\bar{x}) = m_{ij}\, e''(\bar{x}, m) \tag{6}$$

where

$$m_{ij} = \xi_i(m)\,\eta_j(m) + \xi_j(m)\,\eta_i(m) \tag{7}$$

in which $\xi_i(m)$ and $\eta_i(m)$ denote the components of unit vectors along $\xi(m)$ and $\eta(m)$ directions, respectively. It is shown in the appendix that $\int_S \tau^k_{ij}(x,\bar{x})\,\frac{\partial e''(\bar{x},m)}{\partial \bar{x}_\ell}\,d\bar{x}_1\,d\bar{x}_2$ converges uniformly in the slid region S, hence by Equations (1) and (6), the stress at field point x caused by a given plastic strain distribution e"(x, m) in the slid region S is given as

$$\tau_{ij_s}(x) = -2\mu\, m_{kl} \int_S \tau^k_{ij}(x,\bar{x})\,\frac{\partial e''(\bar{x},m)}{\partial \bar{x}_\ell}\,d\bar{x}_1\,d\bar{x}_2 \tag{8}$$

This integral, and hence τ_{ij_s} in the above equation exists and represents a continuous function on S. In equation (8), the repetition of slip system m denotes summation over all sliding slip systems at point x while the subscripts k and ℓ range from 1 to 2. The above discussion holds also when the slid region S is a multi-connected region where the slip strain is continuous inside each simply-connected subregion.

Slip in any region depends on its resolved shear stress. The resolved shear stress in the n^{th} slip system at a field point x, caused by slip throughout the slid region S, is obtained by transforming the stress $\tau_{ij_s}(x)$ given by Equation (8) from the (x_1, x_2) coordinates to the $(\xi, \eta)_n$ coordinates, where $\xi(n)$ is normal to the slip plane and $\eta(n)$ is along the slip direction of the n^{th} slip system at x:

$$\tau_s(x,n) = \frac{1}{2}\, n_{ij}\, \tau_{ij_s}(x) \tag{9}$$

in which n_{ij} is defined by Equation (7). The substitution of Equation (8) into

Equation (9) yields

$$\tau_s(x,n) = -\mu\, m_{k\ell}\, n_{ij} \int_S \tau_{ij}^{k}(x,\bar{x})\, \frac{\partial e''(\bar{x},m)}{\partial \bar{x}_\ell}\, d\bar{x}_1 d\bar{x}_2 \tag{10}$$

Letting $N_\ell(x,n;\bar{x},m) = \frac{1}{2} n_{ij} m_{k\ell}\, \tau_{ij}^{k}(x,\bar{x})$, the above equation may be written in the following form,

$$\tau_s(x,n) = -2\mu \int_S N_\ell(x,n;\bar{x},m)\, \frac{\partial e''(\bar{x},m)}{\partial \bar{x}_\ell}\, d\bar{x}_1 d\bar{x}_2 \tag{11}$$

It is shown in the appendix that the integral in Equation (A-3) over the region $S_\varepsilon(x)$ tends to zero as the radius ε of $S_\varepsilon(x)$ approaches zero. Hence, Equation (11) can be written as:

$$\tau_s(x,n) = -2\mu \int_{S-S_\varepsilon} N_\ell(x,n;\bar{x},m)\, \frac{\partial e''(\bar{x},m)}{\partial \bar{x}_\ell}\, d\bar{x}_1 d\bar{x}_2 + O(\varepsilon^{\ell+1}) \qquad \text{as} \quad \varepsilon \to 0 \tag{12}$$

Since the integrand in the above equation is regular in the integration domain $S - S_\varepsilon$ the area integral can be integrated by parts and partially transformed into a line integral by means of Green's lemma:

$$\begin{aligned}\tau_s(x,n) = &-2\mu \oint_{\Gamma-\Gamma_\varepsilon} [N_1(x,n;\bar{x},m)\, e''(\bar{x},m)\, d\bar{x}_2 - N_2(x,n;\bar{x},m)\, e''(\bar{x},m)\, d\bar{x}_1] \\ &+ 2\mu \int_{S-S_\varepsilon} \left[\frac{\partial}{\partial \bar{x}_1} N_1(x,n;\bar{x},m) + \frac{\partial}{\partial \bar{x}_2} N_2(x,n;\bar{x},m)\right] e''(\bar{x},m)\, d\bar{x}_1 d\bar{x}_2 \\ &+ O(\varepsilon^{\ell+1}) \qquad \text{as} \quad \varepsilon \to 0\end{aligned} \tag{13}$$

where Γ and Γ_ε , taking counterclockwise as positive, denote surfaces bounding the regions S and S_ε respectively. The slip strain in each region of a given slip orientation is taken to be continuous inside and drops to zero at the boundary. The line integral in Equation (13) along Γ vanishes. For numerical calculation, the slid region is divided into thin parallelogram regions unless it is otherwise specified. To simplify calculations, plastic strain in each grid is assumed to be constant. Let S_r denote the region of r^{th} grid, Γ_r the plane surface bounding the grid and

S_o be the grid containing S_ε . Then Equation (13) becomes

$$\tau_s(x,n) = 2\mu e''(\bar{x}_o,m)\oint_{\Gamma_\varepsilon} [\, N_1(x,n,\bar{x},m)\,d\bar{x}_2 - N_2(x,n,\bar{x},m)\,d\bar{x}_1 \,]$$
$$+ 2\mu e''(x_r,m)\int_{\bar{S}_r} \left[\frac{\partial}{\partial \bar{x}_1} N_1(x,n,\bar{x},m) + \frac{\partial}{\partial \bar{x}_2} N_2(x,n,\bar{x},m)\right] d\bar{x}_1\, d\bar{x}_2 \qquad (14)$$
$$+ O(\varepsilon^{p+1}) \qquad \text{as} \quad \varepsilon \to 0$$

In the above, $e''(x_r, m)$ represents the plastic strain due to slip in the m^{th} slip system of the grid $\bar{S}_r$, where

$$\bar{S}_r = S_r - S_\varepsilon\, H(x, x_o) \qquad (15)$$

in which the two-dimensional step unit function $H(x, x_o)$ is defined as

$$\begin{cases} H(x, x_o) = 1 \quad . & \text{if} \quad x \in S_o \\ H(x, x_o) = 0 & \text{if} \quad x \notin S_o . \end{cases}$$

The repetition of r and m denotes summation over all grids S_r and all sliding slip systems at grid centroid x_r. Since the area integrals over the regions $\bar{S}_r$ in Equation (14) are proper, Green's lemma can be applied to reduce area integrals to line integrals. The resulting equation becomes

$$\tau_s(x,n) = 2\mu e''(x_r,m)\oint_{\Gamma_r} [\, N_1(x,n,\bar{x},m)\,d\bar{x}_2 - N_2(x,n,\bar{x},m)\,d\bar{x}_1 \,] \qquad (16)$$

It is clearly seen that the above integral represents the resolved shear stress at x in the n^{th} slip system due to constant unit plastic strain caused by slip in the m^{th} slip system in the region S_r.

If more than one slip system slides at field point x, the plastic resolved shear strain at x in the n^{th} slip system due to slip in different slip systems at the same point x is given as:

$$e''_s(x,n) = \tfrac{1}{2}\, n_{ij}\, m_{ij}\, e''(x,m) \qquad (17)$$

The residual resolved shear stress caused by plastic strain in the slid region S is men:

$$\tau_R(x,n) = \tau_s(x,n) - 2\mu e''_s(x,n) \tag{18}$$

The substitution of Equations (16) and (17) into the above equation yields:

$$\tau_R(x,n) = -2\mu e''(x_r,m)\, G(x,n;x_r,m) \tag{19}$$

where

$$G(x,n;x_r,m) = \frac{1}{2} n_{ij} m_{ij}\, H(x,x_r) - \oint_{\Gamma_r} [N_1(x,n;x_r,m)\,d\bar{x}_2 - N_2(x,n;x_r,m)\,d\bar{x}_1] \tag{20}$$

The function $G(x, n; x_r, m)$ is called the stress influence coefficient of the residual resolved shear stress at x in the n^{th} slip system due to a constant unit plastic strain distribution in the subparallelogram S_r with centroid at x_r, caused by slip in the m^{th} slip system.

The polycrystal is subjected to an alternate tension and compression loading along the x_2-axis as shown in Figure 7. Since the maximum shear stress occurs in a plane at 45° with the direction of loading, the primary slip direction and the normal to the primary slip plane, referred to as the first slip system of the most favorably oriented crystal at the free surface are at 45° with the x_2 -axis:

$$\begin{cases} \xi(1) = (-\frac{1}{\sqrt{2}}, \frac{1}{\sqrt{2}}, 0) \\ \eta(1) = (\frac{1}{\sqrt{2}}, \frac{1}{\sqrt{2}}, 0) \end{cases}$$

It has been pointed out that under cyclic loading, two distinct closely-spaced slices slide. One slice slides during the forward loading, the neighboring slice slides during the reversed loading. The build-up of large local plastic shear strain in the primary slip system in these two thin slices, as shown by Lin and Ito [24, 25], tends to start an extrusion or an intrusion in the region between these slices. Con-

sequently, an appreciable direct stress, tension for extrusion and compression for intrusion, will occur in this region between these slices along the primary slip direction $\eta^{(1)}$. This direct stress gives maximum shear stress along x_1 direction on the x_2 plane, or along x_2 direction on the x_1 plane. A f.c.c. crystal has twelve slip systems. This direct stress causes different resolved shear stresses in the different slip systems. The one with the highest resolved shear stress caused by this direct stress is referred to as the secondary slip system, which should have the slip direction and the normal to the slip plane close to x_1 and x_2 axes. To simplify the numerical calculation, this secondary slip system is assumed to have the slip direction and the normal to the slip plane along x_1 and x_2 axes, i.e.,

$$\begin{cases} \xi^{(2)} = (\ 0,\ 1,\ 0\ ) \\ \eta^{(2)} = (\ 1,\ 0,\ 0\ ) \end{cases}$$

The grids are taken to be rectangles for the secondary slip system in the x_1-x_2 plane, as shown in Figure 8.

To find the stress influence coefficient $G(x, n; x_r, m)$, the surface integral in Equation (16) has to be evaluated. The detail integration of the integral is given by Lin [36]. The resulting expressions are given as follows:

$$\begin{cases} G(x,1;x_r,1) = -K_1(x_1,x_2;x_{1_r}+\frac{a}{2},x_{2_r}+\frac{a}{2}+\frac{b}{2}) + K_1(x_1,x_2;x_{1_r}+\frac{a}{2},x_{2_r}+\frac{a}{2}-\frac{b}{2}) \\ \qquad + K_1(x_1,x_2;x_{1_r}-\frac{a}{2},x_{2_r}-\frac{a}{2}+\frac{b}{2}) - K_1(x_1,x_2;x_{1_r}-\frac{a}{2},x_{2_r}-\frac{a}{2}-\frac{b}{2}) \\ G(x,2;x_r,1) = -K_2(x_1,x_2;x_{1_r}+\frac{a}{2},x_{2_r}+\frac{a}{2}+\frac{b}{2}) + K_2(x_1,x_2;x_{1_r}+\frac{a}{2},x_{2_r}+\frac{a}{2}-\frac{b}{2}) \\ \qquad + K_2(x_1,x_2;x_{1_r}-\frac{a}{2},x_{2_r}-\frac{a}{2}+\frac{b}{2}) - K_2(x_1,x_2;x_{1_r}-\frac{a}{2},x_{2_r}-\frac{a}{2}-\frac{b}{2}) \\ G(x,1;x_r,2) = -K_3(x_1,x_2;x_{1_r}+\frac{\alpha}{2},x_{2_r}+\frac{\beta}{2}) + K_3(x_1,x_2;x_{1_r}+\frac{\alpha}{2},x_{2_r}-\frac{\beta}{2}) \\ \qquad + K_3(x_1,x_2;x_{1_r}-\frac{\alpha}{2},x_{2_r}+\frac{\beta}{2}) - K_3(x_1,x_2;x_{1_r}-\frac{\alpha}{2},x_{2_r}-\frac{\beta}{2}) \\ G(x,2;x_r,2) = -K_4(x_1,x_2;x_{1_r}+\frac{\alpha}{2},x_{2_r}+\frac{\beta}{2}) + K_4(x_1,x_2;x_{1_r}+\frac{\alpha}{2},x_{2_r}-\frac{\beta}{2}) \\ \qquad + K_4(x_1,x_2;x_{1_r}-\frac{\alpha}{2},x_{2_r}+\frac{\beta}{2}) - K_4(x_1,x_2;x_{1_r}-\frac{\alpha}{2},x_{2_r}-\frac{\beta}{2}) \end{cases} \tag{21}$$

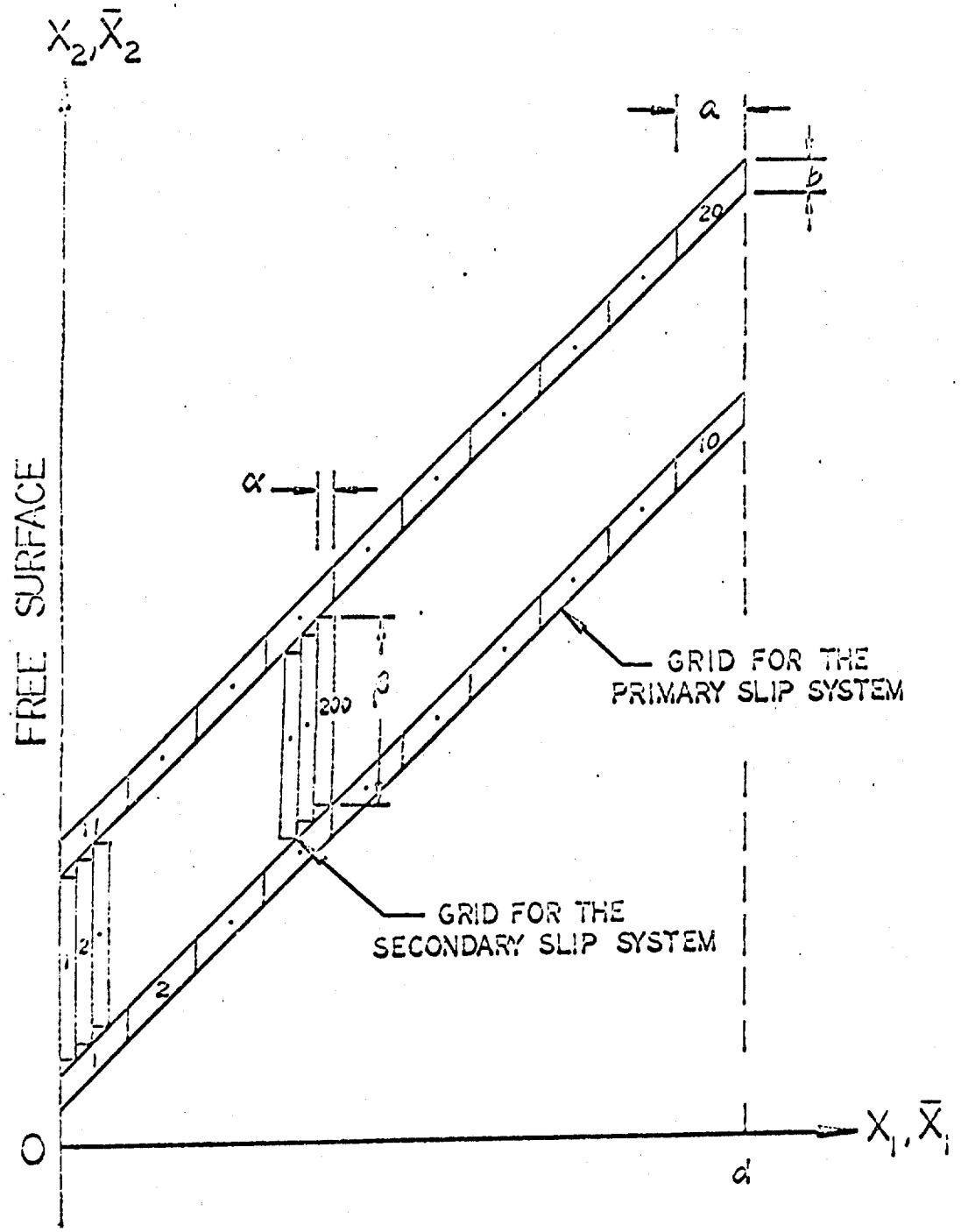

Figure 8. Grids of Primary and Secondary Slip Systems

where

$$\begin{cases} K_1(x_1, x_2; \bar{x}_1, \bar{x}_2) = p\left[-\tan^{-1}\frac{w}{u} + \tan^{-1}\frac{w}{v} + \frac{u(u+w)}{X_1} - \frac{u^2+2uv-v^2+2vw}{2X_2} + \frac{v(v-w)(u^2-v^2)}{X_2^2}\right] \\ K_2(x_1, x_2; \bar{x}_1, \bar{x}_2) = p\left[\frac{1}{2}\log\frac{X_1}{X_2} + \frac{u(u-w)}{X_1} + \frac{u^2+2uw-3v^2}{2X_2} - \frac{v(v+w)(u^2-v^2)}{X_2^2}\right] \\ K_3(x_1, x_2; \bar{x}_1, \bar{x}_2) = p\left[\frac{2u^2}{X_1} - \frac{u^2+2uv-v^2}{X_2} + \frac{2v^2(u^2-v^2)}{X_2^2}\right] \\ K_4(x_1, x_2; \bar{x}_1, \bar{x}_2) = 2pw\left[-\frac{u}{X_1} + \frac{u}{X_2} - \frac{v(u^2-v^2)}{X_2^2}\right] \end{cases} \tag{22}$$

in which

$$\begin{cases} u = x_1 - \bar{x}_1 \\ v = x_1 + \bar{x}_1 \\ w = x_2 - \bar{x}_2 \\ X_1 = u^2 + w^2 \\ X_2 = v^2 + w^2 \end{cases} \tag{23}$$

and, a, b, α and β are the width and thickness of the primary grid and secondary grid, respectively.

When the thickness of grids is much smaller than its width, i.e., $b \ll a$, it can be shown that

$$G(x, l; x_r, l) \doteq 2b\left[K_0(x_1, x_2; x_{1r}+\frac{a}{2}, x_{2r}+\frac{b}{2}) - K_0(x_1, x_2; x_{1r}-\frac{a}{2}, x_{2r}-\frac{b}{2})\right] \tag{24}$$

where

$$K_0(x_1, x_2; \bar{x}_1, \bar{x}_2) = p\left[-\frac{2u}{X_1} + \frac{2u^2(u-w)}{X_1^2} + \frac{2v}{X_2} + \frac{3u^2v+u^2w+2uvw-v^2w-5v^3}{X_2^2} - \frac{4v^2(u^2-v^2)(v+w)}{X_2^3}\right] \tag{25}$$

This clearly shows the linear dependency of the relief of resolved shear stress on the plastic strain and the grid thickness "b". The same result has been pointed out by Lin and Ito [37]. However, the present expression of stress influence co-

efficient is in a much simpler form than that previously given by them.

IV LOCAL PLASTIC STRAIN BUILD-UP UNDER CYCLIC LOADING

The maximum local plastic strain build-up at the free surface is used as the criterion for estimating early fatigue damage. To determine quantitatively this plastic strain build-up for the fatigue nucleation mechanism, the following procedure is used.

Consider a polycrystalline metal with initial resolved shear stress τ_I. This metal is subjected to an alternate stress τ_{ij}. Before slip occurs, the applied resolved shear stress τ_A is uniform. The resolved shear stress at x in the n^{th} slip system due to the applied cyclic stress is

$$\tau_A(x,n) = \frac{1}{2} n_{ij} \tau_{ij_0} = L(x,n)\,\tau_0 \tag{26}$$

where L (x, n) is the Schmid factor which gives the ratio of the resolved shear stress in a particular slip system to the applied load τ_0.

Under the initial forward loading, the resolved shear stress is $\tau_A + \tau_I$. When the critical shear stress is reached, plastic strain occurs and produces residual resolved shear stress as given by Equation (19). The total resolved shear stress in the n^{th} slip system at x is the sum of the applied, initial and residual resolved shear stresses:

$$\tau(x,n) = L(x,n)\,\tau_0 + \tau_I(x,n) - 2\mu G(x,n;x_r,m)\,e^{a}(x_r,m) \tag{27}$$

The repetition of m and r denotes summation over all sliding slip systems in all slid regions. The initial stress field does not change with loading, so that $\frac{d\tau_I(x,n)}{d\tau_0} = 0$. The incremental rate of resolved shear stress with respect to applied load τ_0 is

$$\frac{d\tau(x,n)}{d\tau_0} = L(x,n) - 2\mu G(x,n;x_r,m)\,\frac{de^{a}(x_r,m)}{d\tau_0} \tag{28}$$

Those grids in which the magnitude of the resolved shear stress is less than the critical shear stress τ_c are referred to as non-active slip grids. If R_p is one of these slip grids,

$$| \tau(x_p, n) | < \tau_c \quad , \quad \Delta e''(x_p, n) = 0 \tag{29}$$

where x_p is the centroid of the grid R_p. In the region currently sliding, the magnitude of the resolved shear stress equals the critical shear stress. Let R_S be one of the grids in the sliding region with centroid at x_s. It follows

$$| \tau(x_s, n) | = \tau_c \quad , \quad | \Delta e''(x_s, n) | > 0 \tag{30}$$

where n denotes the sliding slip system at x_s.

The macroscopic plastic strain of the crystal represents the average value in the crystal [12]. Since the slip is highly concentrated in the thin slices, the macroscopic plastic strain is much less than the local plastic strain [24,25]. The rate of strain-hardening in terms of the local plastic strain is hence much less than that in terms of macroscopic strain. To simplify the calculations, this local strain-hardening is neglected. Then Equation (28) gives

$$2\mu\, G(x_s, n; x_r, m)\, \frac{de''(x_r, m)}{d\tau_o} = L(x_s, m) \tag{31}$$

where x_s and x_r denote the centroids of sliding regions. This is a set of linear equations with as many non-zero unknowns $\frac{de''(x_r, m)}{d\tau_o}$ as there are equations. The plastic strain increment $\Delta e''(x_r, m)$ in the sliding grids for an increment of applied stress $\Delta\tau_o$ can readily be determined from the value of $\frac{de''(x_r, m)}{d\tau_o}$. Substitution of $\frac{de''(x_r, m)}{d\tau_o}$ into Equation (28) yields the rate of change of the resolved shear stress at all points. From the known values of $\tau(x, n)$ at the non-active points and the corresponding values of $\frac{d\tau(x, n)}{d\tau_o}$, the increments

in τ_o required for each non-active point to initiate slip can be calculated and compared. The minimum of these required increments in τ_o is applied, resulting in one additional active point for the next load interval. During reversed loading, the incremental aggregate stress in reverse loading required for a new slip region to slide can similarly be found.

It should be noted that the incremental calculation of slip strains and stresses under quasi-static cyclic loading outlined in the foregoing is rigorous within the framework of the discretized formulation. It is also valid for piecewise linear strain-hardening.

The extrusion thickness has been observed to be about 0.1 $m\mu$ (micron) by Forsyth and Stubbington [38], so that the distance between the two slices is taken to be 0.1 $m\mu$. The thickness of the slices P and Q in Figure 8 is very small and is assumed to be 0.01 $m\mu$. The initial stress field in the primary slip system at the free surface is assumed to be zero everywhere except in the two neighboring slices P and Q, in which the initial stress varies linearly with the depth of the slice, i.e.,

$$\tau_I(x,1) = \begin{cases} 5\left(1 - \frac{2x_1}{d}\right) & \text{in P} \\ -5\left(1 - \frac{2x_1}{d}\right) & \text{in Q} \\ 0 & \text{elsewhere} \end{cases}$$

where the linear dimension, d, of the sliding crystal is taken to be 25 $m\mu$. To reduce the lengthly computer calculation, the secondary slip is allowed to slide only in the region between two slices P and Q, and up to a distance 10 $m\mu$ from the free surface. 200 grids within this 10 $m\mu$ distance were taken for this secondary slip calculation. The sliding of the secondary slip system in the interior region between P and Q, and beyond 10 $m\mu$ from the free surface is taken to have little effect on the plastic strain build-up near the free

surface. The relief of the resolved shear stress due to plastic strain in the slid grid is assumed to be given by that at the centroid of the grid. The build-up of local plastic strain in the primary and secondary slip systems is calculated for an applied alternating stress of 100 psi along x_2 -direction. The critical shear stress is taken to be 53.5 psi, the shear modulus μ to be 3.85×10^6 psi and the elastic Poisson's ratio σ to be 0.3. These values correspond approximately to those for pure aluminum [39].

The calculated resolved shear stress distributions under forward loading at the 35th cycle with and without considering the secondary slip are shown respectively in Figures 9 and 10. It is interesting to note that, during fatigue loadings, the difference in the residual resolved shear stresses in the slices P and Q near the free surface is about constant for the case with only primary slip system sliding, while the difference is steadily increased with both primary and secondary slip systems jointly sliding.

The calculated local plastic strain in the primary slip system in the slice P considering sliding in the secondary slip system at various cycles of loading is shown in Figure 11. The local plastic strain reaches approximately 3% at the free surface grid in about 36 cycles. The local plastic strain build-up at the interior end of the thin slice is much slower (only about 1/3) than that at the free surface as predicted by Lin and Ito [40]. Hence, in general, fatigue cracks occur at the free surface before any interior crack has a chance to initiate.

The increase of maximum local plastic strain in the primary slip system at the free surface with and without the sliding of the secondary slip system are shown in Figure 12. The build-up of the plastic strain in the primary slip system with the secondary slip sliding is much faster than that with only primary slip

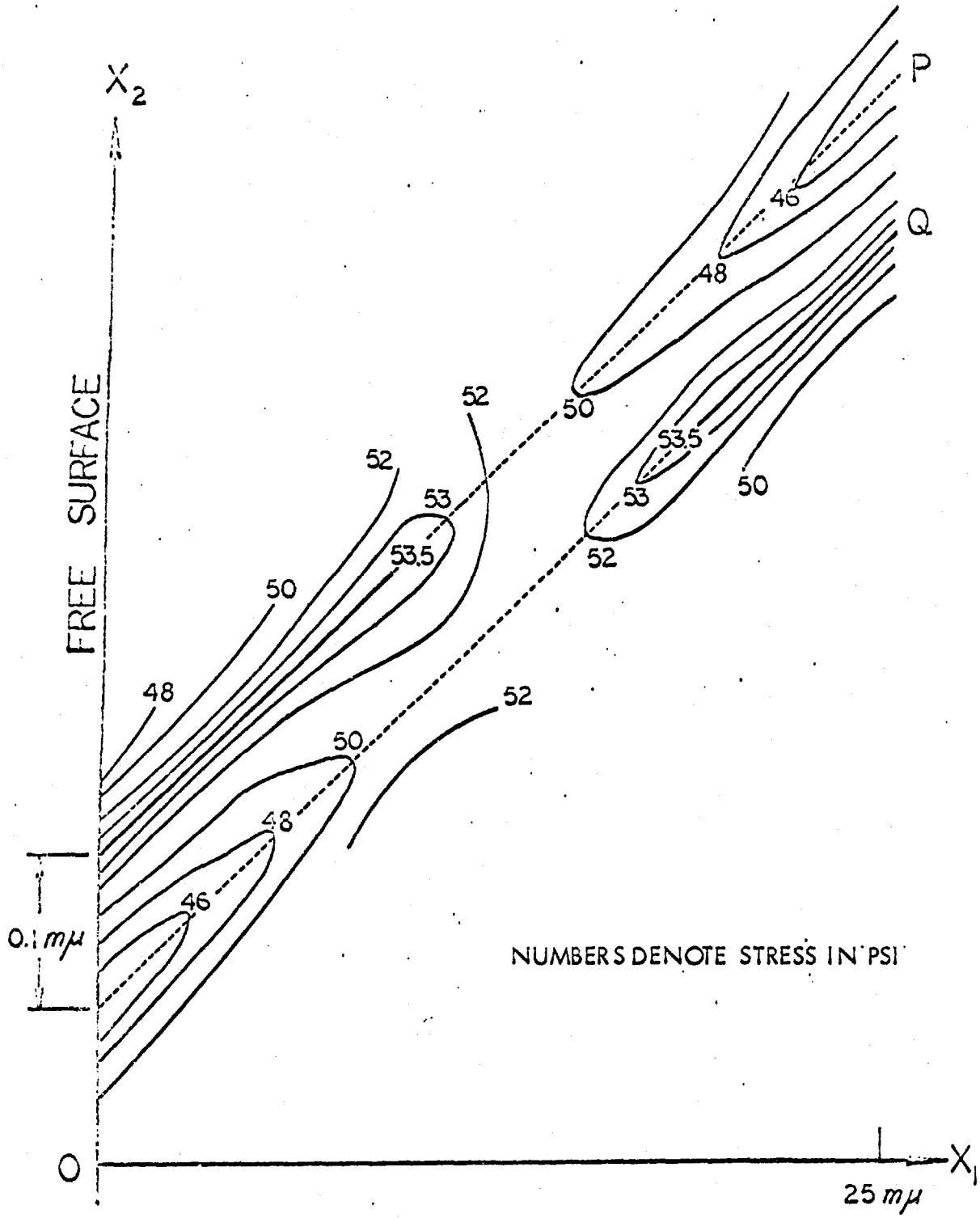

Figure 9. Resolved Shear Stress in the Primary Slip System Under Forward Loading of 35th Cycle without Secondary Slip

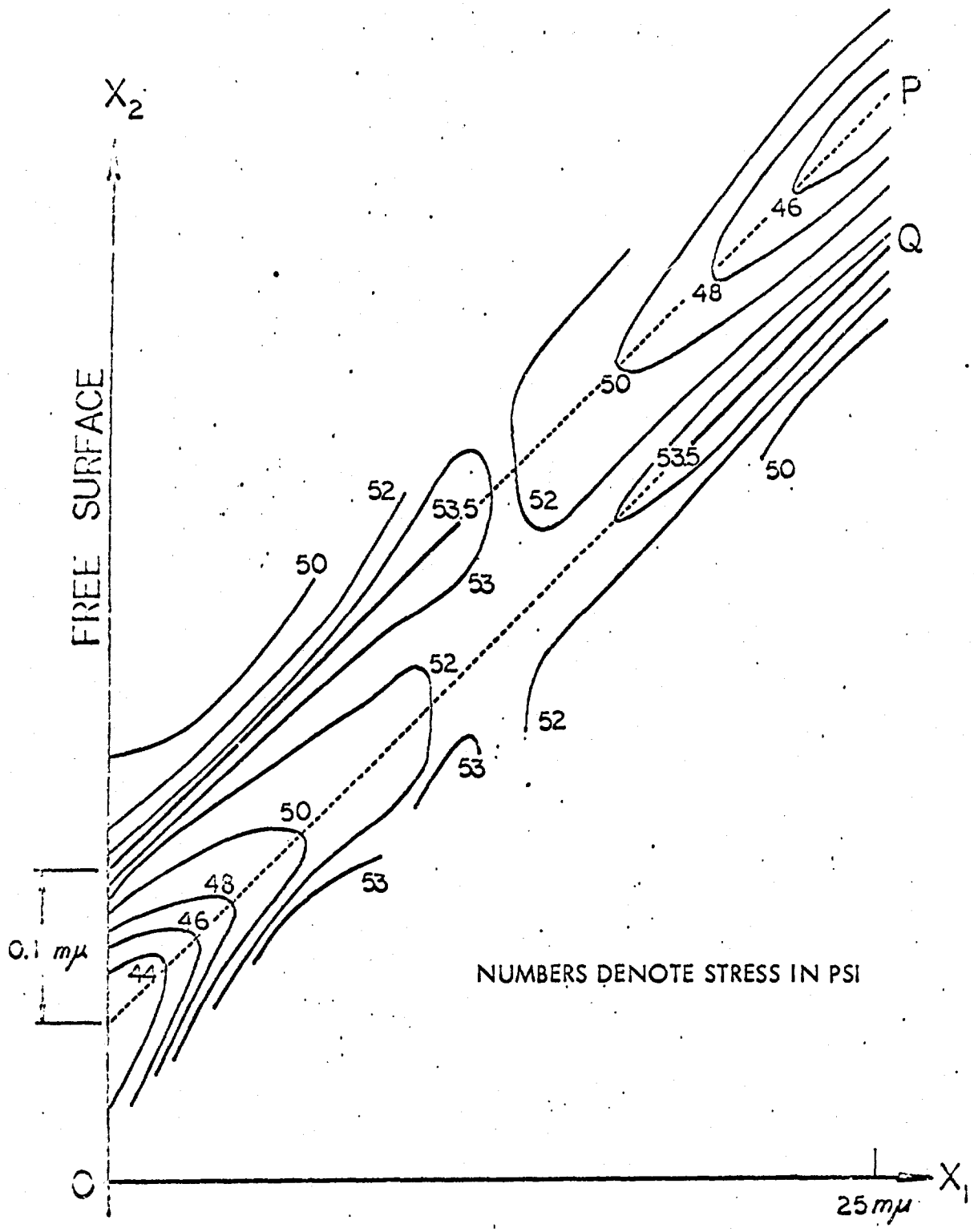

Figure 10. Resolved Shear Stress in the Primary Slip System Under Forward Loading of 35th Cycle with Secondary Slip

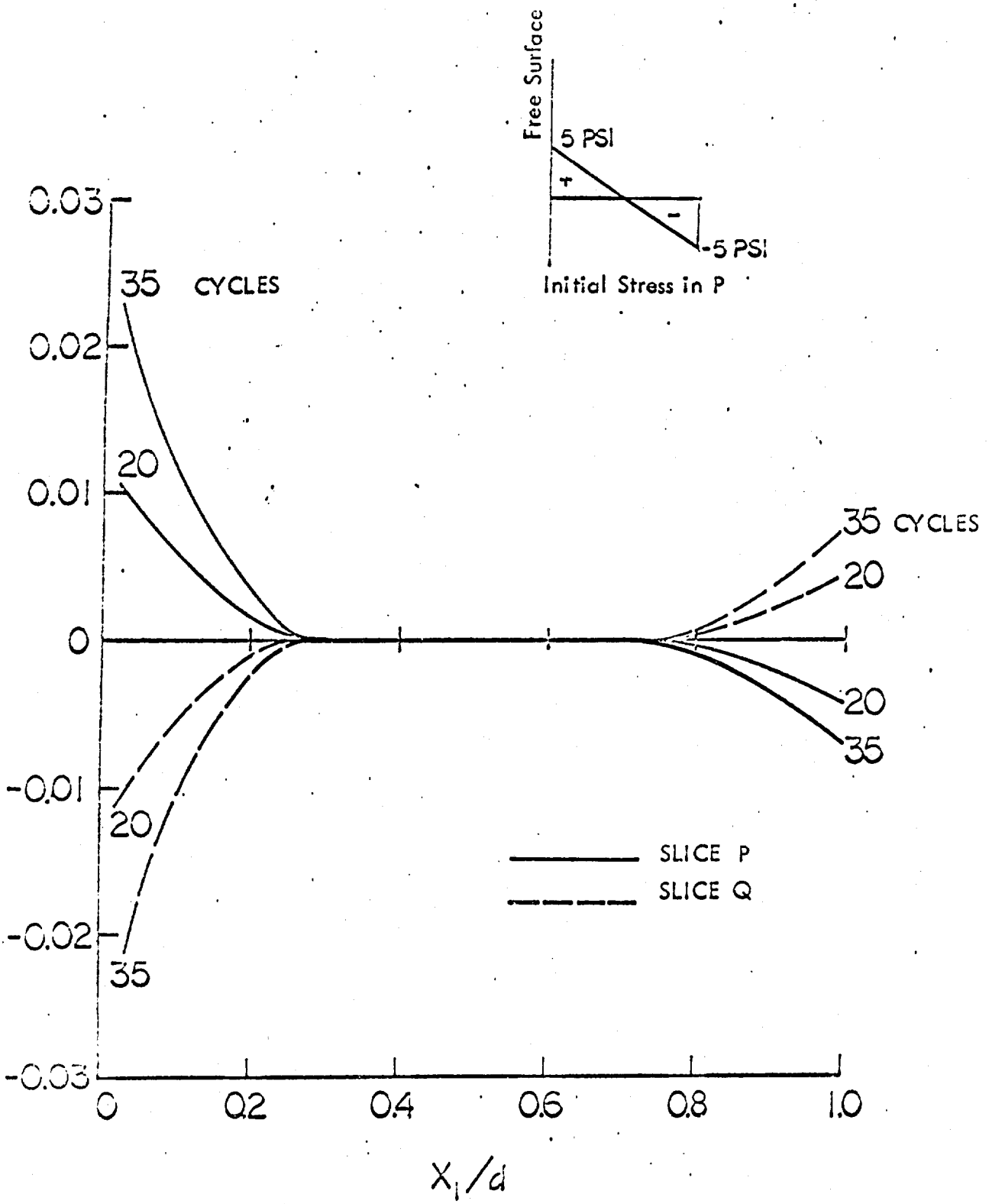

Figure 11. Distribution of Plastic Strain in Sliding Slices

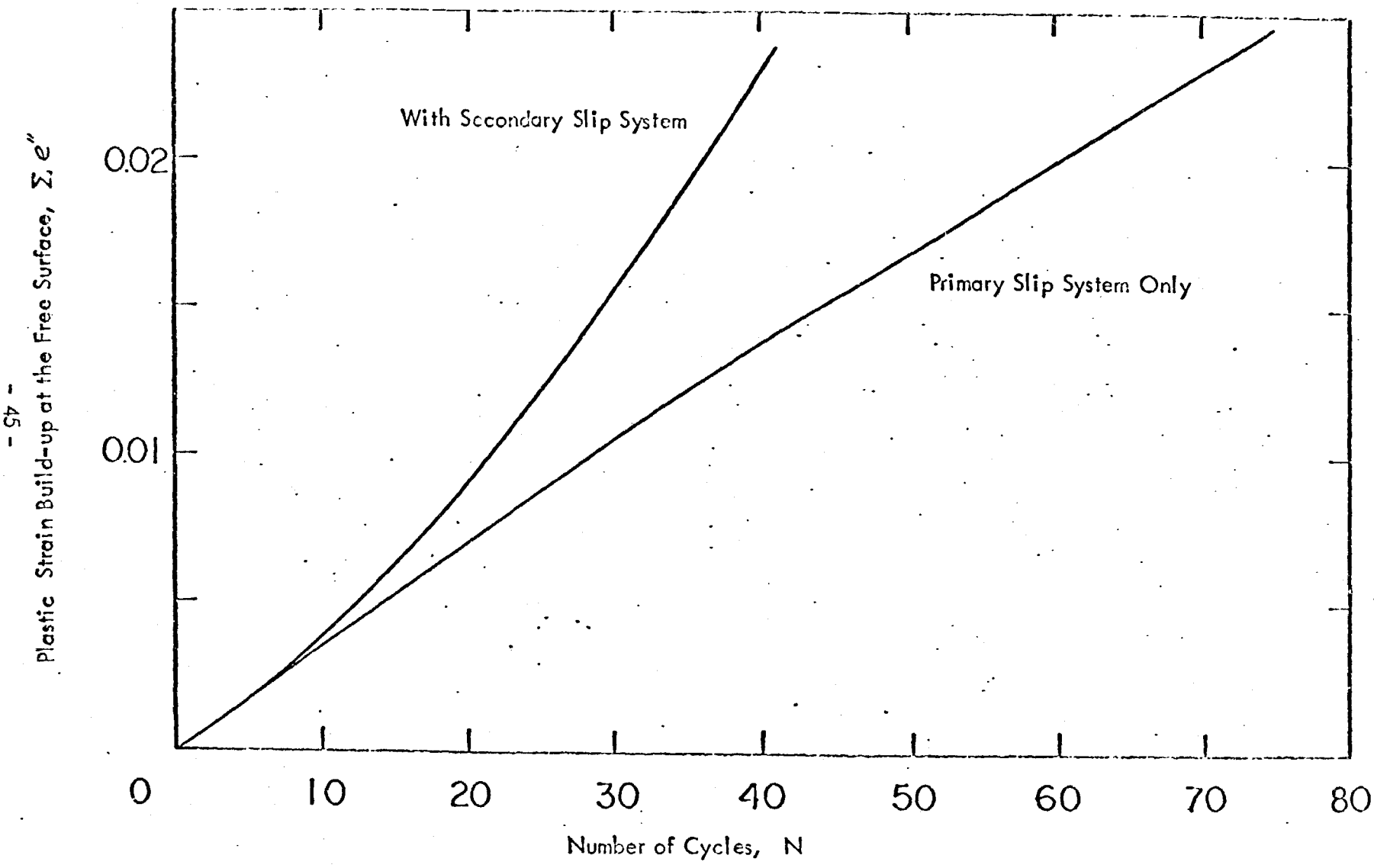

Figure 12. Maximum Local Plastic Strain Build-up at the Free Surface

system sliding. The build-up in the latter case is approximately linear with the number of cycles.

V CONCLUSION

The resolved shear stress field caused by a uniform distribution of plastic shear strain in one grid in a semi-infinite medium was obtained in closed form. This solution in closed form was used to calculate the build-up of local plastic strain at the free surface. The local strain-hardening in the slid region is assumed to be zero. The activation of the second slip system is allowed during the fatigue cycling. Calculated results show that sliding of the primary slip system increases the residual resolved shear stress in the secondary slip system monotonically at a relatively rapid rate and helps the secondary slip system to slide at the early state of fatigue cycling. The slip in the secondary slip system also affect greatly the rate of the local plastic strain build-up in the primary slip system. The build-up of local plastic strain is used as the criterion for estimating early fatigue damage. Hence, the sliding of the secondary slip system increases greatly the rate of fatigue damage. In those regions where two slip systems are active, the total plastic strain is the tensor sum of the slip of the two systems. The amounts of slip in these two systems vary from point to point. The plane of maximum plastic shear strain caused by slip in these two systems varies from point to point. It seems that the variation of the orientation of this plane may cause the waviness of slip lines observed on specimen [41, 42].

The slip distribution calculated by the present analysis satisfy the conditions of compatibility and equilibrium, as well as the dependency of slip on the resolved shear stress throughout the metal for all stages of alternating load.

Part C

Preliminary Evaluation of Plasma Spray Metal Coatings as a Means for Prolonging Fatigue Life

The nucleation of a fatigue crack generally occurs at the free surface due to the large build-up of local plastic strain resulting from slip at the free surface. It was experimentally shown that successive electropolishing the surface of a specimen undergoing fatigue testing will considerably increase the fatigue life. Hence, it appears that the fatigue life of a specimen can be extended if its surface fatigue properties are improved.

One method that may accomplish this is to give the specimen surface a coating which has a higher fatigue life than the specimen itself. This coating must form a strong molecular bond with the specimen. It was thought that some plasma spray coatings might satisfy these requirements. A brief literature survey was made on the effect of plasma spray coating on fatigue life of base material. The results of this survey are briefly summarized as follows.

Plasma spray coatings of Nickel-Aluminide and Carbide types were found to adversely affect the fatigue properties of aluminum alloy 2024-T4 and ultra-high strength steel, AISI type H-11 [43]. The plasma spray process or preparation procedure has little effect on the high cycle endurance limit of aluminum alloy 2024-T4. This agrees with previous work done by Whittaker [44], Remmelts [45], and Wolff [46]. However, there is some low cycle fatigue life reduction. The high cycle endurance limit of high strength H-11 steel heat-treated to 280 ksi tensile strength was found to reduce by 15 to 25 percent by the application of plasma sprayed Nickel-Aluminide and/or Carbide coatings, with corresponding reduction in low cycle fatigue life. The same results were found in the plasma coated titanium 6AL-4V and AISI 9310 steel [47].

The above plasma spray coatings do not have beneficial effects on fatigue. However, the fatigue lives of the coating materials under cyclic strain are not known. The reduction of fatigue life of the base material due to the coating may be caused by the low fatigue life of the coating. From Coffin-Mason's law of fatigue, under low cycle fatigue loadings, ductile materials have longer fatigue life under constant cyclic strain than the less ductile ones. A coating of ductile material well bonded to a less ductile base should increase the fatigue life of the base material. However, such a metallurgical process giving perfect bonding of this coating to such a base material has not been found in the literature. For the improvement of fatigue properties such a process needs to be developed.

REFERENCES

1. Popov, E. P., "Bending of Beams with Creep", J. Applied Physics, Vol. 20, p. 251, 1949.
2. Freudenthal, A. M., The Inelastic Behavior of Engineering Materials and Structures, John Wiley, New York, 1950.
3. LiLove, C., "Creep Buckling of Columns," J. Aerospace Science, Vol. 19, pp. 459-467, 1952.
4. Lin, T. H., "Creep deflections and Stresses of Beam-Columns," J. Applied Mechanics, Vol. 25, pp. 75-78, 1958.
5. Malinin, N. N., "Continuous Creep of Round Symmetrically Loaded Plates," (in Russian), Moskov, Vysshe Technichesscoe Vohilische Truda, Vol. 26, p. 221, 1953.
6. DeLeeuw, S. L. and G. E. Mase, "Behavior of Viscoelastic Plates Under the Action of In-Plane Forces", Proc. 4th U. S. National Congress of Applied Mechanics, pp. 999-1005, 1962.
7. Lin, T. H., "Bending of a Plate with Nonlinear Strain Hardening Creep," Proc. International Union of Theoretical and Applied Mechanics, Springer Verlag, Berlin, pp. 215-228, 1962.
8. Lin, T. H. and J. K. Ganoung, "Bending of Rectangular Plates with Nonlinear Strain-Hardening Creep," Int. J. Mechanical Sciences, Vol. 6, pp. 337-348, 1964.
9. Ho, E. Y. and T. H. Lin, "Creep Bending of Rectangular Plates with Large Deflection", AIAA J., Vol. 8, pp. 1346-1347, 1970.
10. Stricklin, J. A., P. T. Hsu and T. H. H. Pian, "Large Elastic, Plastic and Creep Deflections of Curved Beams and Axisymmetric Shells," AIAA J., Vol. 2, pp. 1613-1620, 1964.

11. Leech, J. W., E. A. Witmer and T. H. H. Pian, "Numerical Calculation Technique for Large Elastic-Plastic Transient Deformations of Thin Shells," AIAA J., Vol. 6, pp. 2352-2359, 1968.

12. Lin, T. H., Theory of Inelastic Structures, John Wiley, New York, 1968.

13. Lackman, L. M., "Circular Plates Loaded into the Plastic Region", J. Engineering Mechanics Division, Proc. ASCE, Vol. 90, EM6, pp. 4155-4157, 1964.

14. Lin, T. H., S. R. Lin and B. Mazelsky, "Elastoplastic Bending of Rectangular Plates with Large Deflection," J. Applied Mechanics, Vol. 39, pp. 978-982, 1972.

15. Reissner, E., "On Axisymmetrical Deformations of Thin Shells of Revolution," Third Symposium of Applied Mathe., pp. 27-52, 1950.

16. Shanley, F. R., Weight-Strength Analysis of Aircraft Structures, McGraw-Hill, New York, 1952.

17. Hill, R., Mathematical Theory of Plasticity, Clarendon Press, Oxford, 1950.

18. Radkowski, P. P., R. M. Davis and M. R. Baldue, "Numerical Analysis of Equations of Thin Shells of Revolution," ARS J., Vol. 32, pp. 36-41, 1962.

19. Budiansky, B. and P. P. Radkowski, "Numerical Analysis of Unsymmetrical Bending of Shells of Revolution," AIAA J., Vol. 1, pp. 1833-1842, 1963.

20. Donnell, L. H., "The Flexibility of Corrugated Pipes Under Longitudinal Forces and Bending," Trans. ASME, Vol. 54, 1932.

21. Clark, R. A. and E. Reissner, "On Axially Symmetric Bending of Nearly Cylindrical Shells of Revolution", J. Applied Mechanics, Vol. 23, pp. 59-67, 1956.

22. Hamada, M., Y. Seguchi, S. Ito, E. Kaku, K. Yamakawa and I. Oshima, "Numerical Method for Nonlinear Axisymmetric Bending of Arbitrary Shell of Revolution and Large Deflection Analysis of Corrugated Diaphram and Bellows, "Bulletin of JSME, Vol. 11, pp. 24-33, 1968.

23. Ewing, J. A. and J. C. W. Humphrey, "The Fracture of Metals Under Alternations of Stress," Phil. Trans. Roy. Soc., Series A, 200:241-250, December 1902.

24. Lin, T. H. and Y. M. Ito, "Mechanics of a Fatigue Crack Nucleation Mechanism," J. Mech. Phys. Solids, 17:511-523, December 1969.

25. Lin, T. H. and Y. M. Ito, "Fatigue Crack Nucleation in Metals," Proc. National Academy of Sciences, 62:631-635, March 1969.

26. Lin, T. H. and Y. M. Ito, "The Influence of Strain-Hardening and Grain Size on Early Fatigue Damage Based on a Micromechanics Theory," J. Mech. Phys. Solids, 19:31-38, January 1971.

27. Lin, T. H. and Y. M. Ito, "A Micromechanics Theory of the Effect of Mean Stress on Fatigue Crack Nucleation," Proc. Air Force Conference on Fatigue and Fracture of Aircraft Structures and Materials, Air Force Flight Dynamics Laboratory, Miami Beach, Florida, December 1969, AFFDL TR 70-144, pp. 63-69, 1969.

28. Kennedy, A. J, "Possible Dislocation Gating Mechanism for Fatigue Extrusion," Phil. Mag., 6:49-53, January 1961.

29. Dorn, J. E. and J. D. Mote, "On Plastic Behavior of Polycrystalline Aggregates," Report UCRL-10152, University of California, Lawrence Radiation Laboratory, 1962.

30. Taylor, G. I. and C. F. Elam, "The Distortion of an Aluminum Crystal During a Tensile Test," Proc. Roy. Soc., Series A, 102:643-667, March 1923.

31. Taylor, G. I. and W. S. Farren, "The Distortion of Crystals of Aluminum Under Compression, Part I", Proc. Roy. Soc., Series A, 111:529-551, February 1926.

32. Reissner, H., "Eigenspannungen und Eigenspannungsquellen," Z. Agnew. Math. Mech., 11:1-8, 1931.

33. Eshelby, J. D., "The Determination of the Elastic Field of an Ellipsoidal Inclusion and Related Problems," Proc. Roy. Soc. A, 241:396, 1957.

34. Melan, E, "Der Spannungszustand der durch eine Einzelkraft in Innern beanspruchten Halbscheibe," Zeitschrift fur Angewandte Mathematik und Mechanik, 12:343-346, December 1932. Correction in 20:368, December 1940.

35. Tung, T. K. and T. H. Lin, "Slip Strains and Stresses in Polycrystalline Aggregates under Cyclic Load," J. Appl. Mech., 29:363-370, June 1966.

36. Lin, S. R., Effect of Secondary Slip Systems on Early Fatigue Damage, PhD. Dissertation, University of California, Los Angeles, 1971.

37. Lin, T. H. and Y. M. Ito, "Mechanism of Fatigue Crack Nucleation Based on Microstresses Caused by Slip," UC-DE-R68-19, University of California, Department of Engineering, Los Angeles, April 1968.

38. Forsyth, P. J. E. and C. A. Stubbington, "The Slip Band Extrusion Effect Observed in Some Aluminum Alloys Subjected to Cyclic Stresses," J. Inst. Met., 83:395-399, April 1955.

39. Wu, T. T, "A Note on the Early Deformation of Aluminum Crystals in Simple Tension," J. Appl. Mech., 31:711-713, December 1964.

40. Lin, T. H. and M. Ito, "Slip Distribution in a Thin Slice of a Crystal at a Free Surface," J. Appl. Phy., 38:775-780, February 1967.

41. Thompson, N. and N. J. Wadsworth, "Metal Fatigue," Advances in Physics, 7:72-170, January 1958.

42. Kennedy, A. J, Processes of Creep and Fatigue in Metals, Oliver and Boyd, Edinburgh, 1962.

43. Meringolo, V., L. Silvaggi and J. Mogul, "The Effect of Plasma Spray Coatings on Fatigue Properties of H-11 Steel and 2024 Aluminum," presented at Sixth International Metal Spraying Conference, Paris, France, 1970.

44. Whittaker, J. A., "Final Report on the Effect of Anodil Metal Coatings on the Fatigue Properties of High Strength Aluminum Alloys," Fulmer Research Institute Ltd. R106/5, 1960.

45. Remmelts, J., "Sprayed Metal Coating for Protection of Bare Aluminum Alloy Parts in Aircraft," NASA N67-10543, 1966.

46. Wolff, F. E., "Airframe Applications of Plasma Sprayed Coatings," presented at Airplanes Plating Forum, Tulsa, Oklahoma, 1969.

47. Meringolo, V., "The Effect of Plasma Spray Coatings on Fatigue Properties of Titanium 6AL-4V and AISI 9310 Steel, "CWC Metallurgical Report B-725, Curtiss-Wright Corporation, Woodridge, New Jersey, 1971.

APPENDIX

Let the plastic strain gradient in slid region S be written as:

$$\frac{\partial e''(\bar{x},m)}{\partial \bar{x}_i} = O(|x-\bar{x}|^{\rho}) \quad \text{for} \quad x \in S \quad \text{as} \quad x \to \bar{x} \qquad (A\text{-}1)$$

where ρ is a real number. For $\rho=-1$, $e''(\bar{x},m)$ would give a logarithmic singularity and becomes infinite as x approaches $\bar{x}$. Consider plastic strain as caused by the displacement of dislocations. Let the lattice spacing be denoted by "A" which is a finite distance. The change of plastic strain across "A" is always finite. Hence $\frac{\partial e''(\bar{x},m)}{\partial \bar{x}_i}$ is bounded and ρ in Equation (A-1) is greater than zero. The stress Green's function $\tau_{ij}^{k}(x,\bar{x})$ at x due to a unit force acting at $\bar{x}$ along x_k direction has been shown to be related to the stress function (Equation 3). It is easily observed through the expressions for the stress function that

$$\tau_{ij}^{k}(x,\bar{x}) = O(|x-\bar{x}|^{-1}) \quad \text{for} \quad x \in S \quad \text{as} \quad x \to \bar{x} \qquad (A\text{-}2)$$

Let $S_\varepsilon(x)$ be a sphere on (x_1, x_2) plane, centered at x with radius ε. It can be shown from Equations (A-1) and (A-2) that for $x \in S_\varepsilon(x)$

$$\int_{S_\varepsilon(x)} \tau_{ij}^{k}(x,\bar{x}) \frac{\partial e''(\bar{x},m)}{\partial \bar{x}_l} d\bar{x}_1 d\bar{x}_2 = O(\varepsilon^{\rho+1}) \to 0 \quad \text{as} \quad \varepsilon \to 0 \qquad (A\text{-}3)$$
$$k, l = 1, 2$$

This integral approaches zero for $\rho > -1$. Since $\rho > 0$, this integral vanishes as $\varepsilon \to 0$. Even though the stress Green's function $\tau_{ij}^{k}(x,\bar{x})$ is singular at $x = \bar{x}$, the integral $\int_S \tau_{ij}^{k}(x,\bar{x}) \frac{\partial e''(\bar{x},m)}{\partial \bar{x}_l} d\bar{x}_1 d\bar{x}_2$ converges uniformly in the slid region S.